

University of Tartu

Faculty of Science and Technology

Institute of Technology

Ikechukwu OFODILE

**Design and Comparison of Attitude Control
Modes for ESTCube-2**

Master's Thesis (30 ECTS)

(Robotics and Computer Engineering)

Supervisors:

Dr. Andris SLAVINSKIS

Assoc. Prof. Gholamreza ANBARJAFARI

Tartu 2017

Contents

Contents	i
List of Figures	iv
List of Tables	vi
Abbreviations	vii
Symbols	viii
1 Introduction	3
1.1 Motivation	3
1.2 Background and Literature Survey	4
1.3 Aim and Objectives	6
1.4 Thesis Outline	6
2 Background to Spacecraft	
Attitude Control	8
2.1 Introduction	8
2.2 Reference Frame	8
2.2.1 Earth-Centered Inertial Reference Frame (ECIF)	9
2.2.2 Earth-Centered Earth Fixed Reference frame (ECEF)	9
2.2.3 Local-Vertical Local-Horizontal Reference frame (LVLH)	9
2.2.4 Spacecraft Body Reference frame (SBRF)	9
2.3 Attitude Parameterization	10
2.3.1 Direction Cosine Matrix (DCM)	10
2.3.2 Euler Angles	10
2.3.3 Unit Quaternions	12
2.3.4 Quaternion Rotation	13
2.3.5 Error Quaternion	14
2.4 Sensors	15
2.4.1 Gyroscopes	15
2.4.2 Accelerometers	15

2.4.3	Magnetometers	16
2.4.4	Sun sensor	16
2.4.5	Star tracker	16
2.5	Actuators	16
2.5.1	Reaction Wheels	16
2.5.2	Magnetic Coils	17
2.5.3	Cold Gas Thruster	18
3	Spacecraft Modeling	19
3.1	Kepler And Newton's Laws	19
3.2	Inertia Matrix	20
3.3	Environmental Models	21
3.3.1	Earth's Geomagnetic Field	21
3.3.2	Gravity-Gradient Torque	23
3.3.3	Aerodynamic Torque	24
3.3.4	Solar Radiation Torque	25
3.3.5	Residual Magnetic Torque	25
3.4	Dynamics	26
3.5	Kinematics	27
3.6	Linearization	28
4	Attitude Control for ESTCube-2	31
4.1	Description and Control Specifications for ESTCube-2	31
4.2	Detumbling Controller Designs	31
4.2.1	B-dot Controller Design	32
4.2.2	P Controller Designs	33
4.2.3	PD Controller Designs	34
4.3	Pointing Controller Designs	34
4.3.1	PD Controller	35
4.3.2	Linear Quadratic Regulator Design	35
4.4	Cross Product Control Law	39
4.5	Spin-up Controller Designs	39
5	Simulation Results and Controller Comparison	43
5.1	B-dot Controller Analysis	43
5.2	PD Controller Analysis	43
5.2.1	PD performance with Magnetorquers	44
5.2.2	PD performance with saturated Reaction Wheels	48
5.2.3	PD performance with unsaturated wheels	51
5.3	Cross Product Control Analysis	54
5.4	LQR Analysis	57
5.5	Spin-up Controller Analysis	62
6	Conclusion & Future Work	65

6.1	Conclusion	65
6.2	Future Work	66
A	Controllability Analysis	71
B	Linear Programming Code.	72
C	Nadir Pointing Satellite Model With Reaction Wheels	75
C.1	Model with Reaction Wheels	75
C.2	Model with Magnetorquers	76
D	Abstracts Accepted for Oral Presentations	78
D.1	Abstract for 68th International Astronautical Congress 2017 - <i>Tether Deployment Using High Spin Rate Control For Interplanetary Nanosatel- lite Missions</i>	78
D.2	Abstract for 6th iCubeSat Workshop 2017 - <i>ESTCube-2 Nanosatel- lite Attitude Control for Interplanetary Missions</i>	79

List of Figures

1.1	ESTCube-2 exploded view [1].	5
3.1	Earth's Magnetic Dipole [2].	22
4.1	Attitude Control block diagram with feedback.	35
4.2	LQR design from linearization.	37
4.3	LQR controller on nonlinear spacecraft model.	37
4.4	LQR controller design algorithm.	38
5.1	Detumbling of Satellite with Bdot Control	44
5.2	Quaternion Attitude during detumbling phase.	44
5.3	Magnetorquer Torque response during detumbling phase.	45
5.4	PD controller Angular velocity for Detumbling/Pointing with Magnetorquer.	46
5.5	PD controller Quaternion Attitude for Detumbling/Pointing with Magnetorquer	46
5.6	Magnetorquer Torque response.	47
5.7	PD controller Angular velocity for Detumbling/Pointing with reaction wheels saturated	48
5.8	PD controller Quaternion Attitude for Detumbling/Pointing with reaction wheels saturated	49
5.9	Angular momentum showing reaction wheels saturated	49
5.10	Reaction Wheel saturated torque response	50
5.11	PD controller Angular velocity for Detumbling/Pointing with reaction wheels	51
5.12	PD controller Quaternion Attitude for Detumbling/Pointing with reaction wheels	52
5.13	Angular momentum showing reaction wheels	52
5.14	Reaction Wheel torque response	53
5.15	Angular velocity response while unloading Reaction Wheels with magnetorquers	54
5.16	Quaternion Attitude during Reaction Wheel unloading with Magnetorquers	55

5.17	Reaction Wheels angular momentum saturated and unloading with magnetorquers	55
5.18	Reaction Wheel torque response during unloading	56
5.19	Magnetorquer torque response with Reaction Wheel unloading	56
5.20	Quaternion Step response (weighting matrices $Q = \text{diag}[1,1,1,1,1, 1]$, $R = \text{diag}[1, 1, 1]$)	58
5.21	Angular Velocity Step response (weighting matrices $Q = \text{diag}[1,1,1,1,1, 1]$, $R = \text{diag}[1, 1, 1]$)	58
5.22	Angular Velocity LQR controller performance with noise.	59
5.23	Quaternion Attitude LQR controller response with noise.	59
5.24	Angular Velocity LQR controller performance.	60
5.25	Angular Velocity LQR controller performance with Magnetorquers.	60
5.26	Quaternion Attitude LQR controller response with Magnetorquers.	61
5.27	Magnetorquer Torque response with LQR.	61
5.28	Angular Velocity Spin up to 110 deg/s.	63
5.29	Angular Velocity Spin up to 180 deg/s.	63
5.30	Angular Velocity Spin up to 360 deg/s.	64

List of Tables

5.1	PD Performance Overview.	45
5.2	Satellite Parameters to obtain LQR controller gain.	57
5.3	Spin rate simulation result.	62
6.1	Overview of Designed Controllers.	65

Abbreviations

ADCS	Attitude Determination and Control System
ACS	Attitude Control System
COM	Communication
EPS	Electrical Power System
ECIF	Earth Centered Inertial Reference Frame
LVLH	Local Vertical Local Horizontal
SBRF	Spacecraft Body Reference Frame
LEO	Low Earth Orbit
GEO	Geosynchronous Earth Orbit
MT	Magnetorquer
RW	Reaction Wheel
PID	Proportional Integral Derivative
LQR	Linear Quadratic Regulator

Symbols

\hat{e}	axis directional unit vector	
$\Omega()$	skew-symmetric cross-product matrix	
a	distance	m
b	Earth's Magnetic Field vector	T
μ_f	Earth's magnetic field's dipole strength	$Wb \cdot m$
h	Angular momentum	$N \cdot m \cdot s$
h_e	Angular momentum error	$N \cdot m \cdot s$
J	Moment of Inertia matrix	$kg \cdot m^2$
m	Magnetorquer dipole vector	$A \cdot m^2$
T	Orbital period	s
ω_i	Inertial Angular velocity	rads^{-1}
ω_o	Orbital Angular velocity	rads^{-1}
T_c	Control Torque	$N \cdot m$
T_d	Disturbance Torque	$N \cdot m$
cp	Centre of Pressure	
cg	Centre of Mass	

UNIVERSITY OF TARTU

Abstract

Faculty of Science and Technology

Institute of Technology

Master of Science

Design and Comparison of Attitude Control Modes for ESTCube-2

by Ikechukwu OFODILE

This thesis presents the attitude control problem of ESTCube-2. ESTCube-2 is a 3U CubeSat with a size of 10 x 10 x 30 *cm* and a weight of about 4 *kg*. It is the second satellite to be developed by the ESTCube Team and will be equipped with the E-Sail payload for the plasma break experiment, Earth observation camera, a high speed communication system, and a cold gas propulsion module. The satellite will make use of 3 electromagnetic coils, 3 reaction wheels and the cold gas thruster as actuators.

The primary purpose of this work was to develop and compare control laws to fulfill the attitude control requirements of the ESTCube-2 mission. To achieve this, the spacecraft dynamics and environmental models are derived and analyzed. PD like controllers and LQR optimal controls are designed to fulfill the pointing requirements of the satellite in addition to the B-dot detumbling control law. Angular rate control law to spin up the satellite for tether deployment is also derived and presented. Simulations of the different controllers shows the performance with disturbances also added to the system. Finally recommendations and optimal control situations are presented based on the results.

Keywords: *CubeSat, ESTCube-2, Attitude Control, High spin rate, LQR.*

CERCS: *P170, T125, T320*

Abstract**ESTCube-2 asendi kontrolli režiimide disain ja võrdlus**

See töö esitab ESTCube-2 asendi kontrolli probleemi. ESTCube-2 on 3U CubeSat, mille suurus on 10x10x10 cm ning selle kaaluks on 4 kg. See on teine satelliit valmistatud ESTCube meeskonna poolt ning selle pardal on erinevad kasulikud lastid: plasma pidur, kaks maavaatluskaamerat, kommunikatsioonisüsteem suurte mateks andmevahetuskiirusteks ning külma gaasi tõukur. Satelliit kasutab asendi kontrollimiseks kolme elektromagnetmähist, kolme reaktsiooniratast ning külma gaasi tõukurit.

Töö peamine eesmärk oli arendada ning võrrelda erinevaid asendi kontrolli algoritme, mis täidaksid ESTCube-2 missiooni nõuded. Selle saavutamiseks tuletati ning analüüsiti satelliidi dünaamika ning keskkonna mudeleid. B-dot pöörlemise vähendamiseks ning suunamise kontrolliteks arendati PD-regulaatoril ning LQ-regulaatoril põhinevaid kontrollereid. Tuletati ning esitati pöörlemiskiiruse kontrollimise seadused, et satelliiti pöörlema panna. Viidi läbi simulatsioonid, millele on lisatud erinevad häired, iseloomustavad süsteemi toimimist. Lõpetuseks antakse töös soovitusel ning optimaalsed kontrolli olukorrad, mis põhinevad eelnevatel tulemustel

Keywords: *CubeSat, ESTCube-2, Attitude Control, High spin rate, LQR.*

CERCS: *P170, T125, T320*

1 Introduction

1.1 Motivation

Since its inception in 2008, the ESTCube project is a student project which is now aimed at getting students involved in understanding the concepts of space technology and its emerging technologies with scientific and engineering impacts. The ESTCube-1 student satellite project was launched on the 7 May 2013, and involved students from the University of Tartu, Estonian Aviation Academy, Tallinn University of Technology and Estonian University of Life Sciences as well as instructors and experts from different countries [3]. The main mission of the ESTCube-1 satellite was to test the Electric Solar wind sail (E-sail) developed by Pekka Janhunen [4]. Students had the opportunity to write their Bachelors' and Masters' Thesis on various parts and subsystems of the satellite including the ADCS, EPS, COM etc. As a student of the Robotics and Computer Engineering Master's Program of the University of Tartu, this thesis will show forth the knowledge I have gained by participating in the ESTCube-2 project relating to spacecraft dynamics and implementation using quaternions as well as controllers to be used on the satellite for attitude control.

1.2 Background and Literature Survey

The increased research interests and innovations in space technology and exploration, has driven a increase in development of nanosatellites (mass of 1-10kg) and microsatellites. These satellites are mostly deployed in Low Earth Orbit (LEO) for various mission objectives such as weather forecasting, telecommunications, earth observation, environmental and scientific research purposes. The development of CubeSat class of nanosatellites, began in 1999 in California [5]. A great success was achieved in a collaborative effort between California Polytechnic State University and Stanford university to develop an efficient and inexpensive satellite. CubeSats have now recently being used as a great opportunity for researchers and universities to advance on the wide range of experimental and research opportunities in space technology.

Satellites deployed for various missions have to be equipped with a reliable Attitude Control System (ACS) to meet the requirements of the mission. Hence the ADCS is regarded as an important subsystem of satellites. It is often expressed as visual perspective or feeling of the satellites in space. The ACS performs several operational modes and must maintain the attitude control even in the presence of disturbance torques on the satellite.

Several works and university thesis reports have aimed to address varying attitude determination and control design objectives and problems. While earlier works are based on euler angle model, recent designs have discussed the design with quaternion models [6–11]. Quaternion applications have been widely used in field of computer science in areas of robotics, computer vision, motion planning, swarm robotics. The use of quaternions in spacecraft model has significant advantage over the Euler angle representation. The quaternion attitude representation, does not depend on rotation sequence as in the case of Euler angle representation, and does not have a singular point for any attitude. This advantages will be described in this thesis work.

The application of Lyapunov based functions to design varying control laws have



FIGURE 1.1: ESTCube-2 exploded view [1].

been presented in [12–14] which may however not be efficient in globally stabilizing the nonlinear complex system. The authors in [15] designed a linearized model with quaternion component as state variables for the nonlinear system implementation. Yang [16] proved the controllability of the linearized quaternion model which globally stabilizes the nonlinear spacecraft model.

The ESTCube-2 ADCS hardware prototype has been designed [17] and currently being developed. The ADCS will contain algorithms which are designed with specific model and requirements to satisfy its mission requirements. As such the algorithms are designed, explained, evaluated and interpreted based on requirements.

1.3 Aim and Objectives

The long term goal and objective of this current study is to give a comprehensive review of ESTCube-2 project relating to spacecraft dynamics and implementation using quaternions as well as controllers to be used on the satellite for attitude control. Spacecraft attitude control system is defined herein as consisting of sensors, attitude actuators and processor which houses the controllers for effective attitude maneuvers. This study will outline the following sub-objectives:

- An overview of the fundamentals in attitude determination and control
- Explain concepts of different reference frame sensors and actuators used
- To derive mathematically the kinematics and dynamics of the satellite
- Elucidate basic attitude control requirements.

The results gotten from this study will be of great significance to the industry practitioners as well as other students involved in ESTCube project.

1.4 Thesis Outline

The rest of the thesis is described as follows

- **Chapter 2** presents the background to spacecraft attitude control, discussing reference frames used in spacecraft attitude determination and control as well as discussing parameters used in attitude representation. Brief discussion on the sensors and actuators used on ESTCube-2 is also presented here.
- **Chapter 3** presents the satellite model describing the satellite dynamics and kinematics as well as its linearized model. Environmental disturbance torques are also discussed as it affects the ESTCube-2 satellite.

-
- **Chapter 4** describes in detail the attitude controllers designed based on the attitude control modes and the set requirements
 - **Chapter 5** presents the simulation results of the controllers designed based on specifications and provides analysis.
 - **Chapter 6** includes the conclusion of the thesis and future work to improve the controllers designed.
 - **Appendix D** Abstracts based on the work done in this thesis accepted for oral presentation at 68th International Astronautical Congress to be held from 25-29 September 2017 in Adelaide, Australia and at the 6th Interplanetary CubeSat Workshop to be held on 30-31 May 2017 at Cambridge, UK.

2 Background to Spacecraft

Attitude Control

2.1 Introduction

Spacecraft attitude control system typically consists of sensors, attitude actuators and processor which houses the controllers for effective attitude maneuvers. In this chapter, I will give an overview of the fundamentals in attitude determination and control, thus explaining concepts as the different reference frames, sensors and actuators used.

2.2 Reference Frame

In Aerospace related applications, many reference frames are used to represent various rotations and concepts, however for the purpose of this report, I will give a brief description of the most important reference frames used in the satellite representations.

2.2.1 Earth-Centered Inertial Reference Frame (ECIF)

The Earth-Centered Inertial Reference Frame (ECIF) is centered in the Earth's center. It is a non rotating reference frame that employs the Newton's laws of motion and gravity on the spacecraft. For inertial pointing spacecrafts, this reference frame is quite important in for use. The x-axis points toward the point where the plane of the Earth's orbit toward Sun, crosses the Equator going from South to North, z-axis points toward the North pole and y-axis completes the right hand Cartesian coordinate system.

2.2.2 Earth-Centered Earth Fixed Reference frame (ECEF)

The Earth-Centered Earth Fixed Reference frame (ECEF) has its origin at the center of the Earth. The x-axis is the direction axis pointing towards the intersection between the Greenwich Meridian and the Equator which is at 0° longitude and 0° latitude. The z-axis is the direction from the center of the Earth pointing to the north pole. The y-axis is the direction that completes the right handed system.

2.2.3 Local-Vertical Local-Horizontal Reference frame (LVLH)

The Local-Vertical Local-Horizontal Reference frame or Orbit frame is most desired for use by many satellites as the z-axis direction points towards the center of the Earth which is a desired nadir pointing mode of satellites. The origin of orbit frame coincides with the center of mass of the satellite. The x-axis is in the direction of the spacecrafts' motion and is perpendicular to the z-axis. The y-axis completes the right handed system.

2.2.4 Spacecraft Body Reference frame (SBRF)

The Spacecraft Body Reference Frame has its origin from the centre of mass of the satellite. In this reference frame, the x-axis is orthogonal to the z-axis and the

y-axis completes the right-handed orthogonal coordinate reference system. During the nadir pointing phase of the satellite, the SBRF and the LVLH reference frames are assumed to be aligned with each other without a rotation about the z-axis.

2.3 Attitude Parameterization

2.3.1 Direction Cosine Matrix (DCM)

The DCM represents the attitude in a 3×3 transformation matrix. This is described by the vector dot product between two coordinate axes representing the cosine of the deviation in angle.

$$A = \begin{bmatrix} u \cdot x & u \cdot y & u \cdot z \\ v \cdot x & v \cdot y & v \cdot z \\ w \cdot x & w \cdot y & w \cdot z \end{bmatrix} \quad (2.1)$$

This DCM is not directly applicable in space missions in representations of attitude as deviations between two coordinate systems is not directly visible or applied to attitude calculations or representations. The Euler angle described next is more applicable.

2.3.2 Euler Angles

The Euler angle representation describes one coordinate frame to another in three successive rotations. This implies a multiplication of three rotation matrices obtained from rotations about three fixed axes. These successive rotations are defined as roll, pitch and yaw, where the roll angle ρ is a rotation about the x-axis, the pitch angle θ about the y-axis and the yaw angle ψ about the z-axis. The rotation matrices are defined as follows

The rotation (axis transformation) matrices are given as:

$$R_z = \begin{bmatrix} \cos \psi & \sin \psi & 0 \\ -\sin \psi & \cos \psi & 0 \\ 0 & 0 & 1 \end{bmatrix} \quad (2.2)$$

$$R_y = \begin{bmatrix} \cos \theta & 0 & -\sin \theta \\ 0 & 1 & 0 \\ \sin \theta & 0 & \cos \theta \end{bmatrix} \quad (2.3)$$

$$R_x = \begin{bmatrix} 1 & 0 & 0 \\ 0 & \cos \phi & \sin \phi \\ 0 & -\sin \phi & \cos \phi \end{bmatrix} \quad (2.4)$$

R_z is the transformation matrix for a fixed point about the z axis.

R_y is the transformation matrix for a fixed point about the y axis.

R_x is the transformation matrix for a fixed point about the x axis.

The resultant transformation matrix from inertial to body frame is given as

$$R = R_z \cdot R_y \cdot R_x$$

$$R = \begin{bmatrix} \cos \psi & \sin \psi & 0 \\ -\sin \psi & \cos \psi & 0 \\ 0 & 0 & 1 \end{bmatrix} \begin{bmatrix} \cos \theta & 0 & \sin \theta \\ 0 & 1 & 0 \\ -\sin \theta & 0 & \cos \theta \end{bmatrix} \begin{bmatrix} 1 & 0 & 0 \\ 0 & \cos \phi & -\sin \phi \\ 0 & \sin \phi & \cos \phi \end{bmatrix}$$

$$R = \begin{bmatrix} C\theta \cdot C\psi & C\psi \cdot S\theta \cdot S\phi - C\phi \cdot S\psi & C\psi \cdot S\theta \cdot C\phi - S\phi \cdot S\psi \\ C\theta \cdot S\psi & S\psi \cdot S\theta \cdot S\phi - C\phi \cdot C\psi & S\psi \cdot S\theta \cdot C\phi - S\phi \cdot C\psi \\ -S\theta & C\theta \cdot S\phi & C\phi \cdot C\phi \end{bmatrix} \quad (2.5)$$

The elements C() and S() are used as an abbreviation for the trigonometric expression cos() and sin() respectively.

2.3.3 Unit Quaternions

Quaternions are referred to as hyper complex numbers and was first introduced by mathematician Rowan Hamilton in the early 19th century and over time have been applied to mechanics solutions. Quaternions are used to express a rotation by a rotational angle about an axis unlike Euler angles which represents rotations by a series of rotations about x, y or z axes. The rotation performed by quaternions are not explicitly about an x, y or z axes. Just like complex numbers, quaternions have basis i, j, k satisfying the following expression

$$i^2 = j^2 = k^2 = -1 = ijk \quad (2.6)$$

Therefore we can define quaternions as follows representing an addition of both scalar and vector component.

$$q = iq_1 + jq_2 + kq_3 + q_0 \quad (2.7)$$

Thus quaternions contains four numbers and for simplicity in expressions, q_0 is the scalar part of the quaternions and the vector component is represented as

$$q_v = iq_1 + jq_2 + kq_3 \quad (2.8)$$

The normalized quaternion is therefore represented as

$$q_0 = \cos(\theta/2) \quad (2.9)$$

$$q_v = \hat{e} \sin(\theta/2) \quad (2.10)$$

where

- \hat{e} is the rotational axis,

- θ is the angle of rotation.

The author in [18] defined and derived the multiplication of two quaternions in order to obtain the quaternion rotation as follows

$$a \otimes b = a_0 b_0 - a_v b_v + a_0 b_v + b_0 a_v + a \times b \quad (2.11)$$

In recall of complex conjugates, the quaternion complex conjugate can be represented as

$$q^* = q_0 - q_v = q_0 - iq_1 - jq_2 - kq_3 \quad (2.12)$$

Therefore the norm of a quaternion can then be defined easily as

$$\|q\| = \sqrt{q^* \otimes q} \quad (2.13)$$

$$\|q\| = \sqrt{q_0^2 + q_1^2 + q_2^2 + q_3^2} = 1 \quad (2.14)$$

The inverse of a normalized quaternion satisfying the above equation is

$$q^{-1} = q^* \quad (2.15)$$

2.3.4 Quaternion Rotation

In order to obtain the quaternion rotation operator, we make use of the normalized quaternion defined in Equations 2.9 and 2.10. Therefore we express the quaternion as

$$q = q_0 + q_v = \cos\left(\frac{\theta}{2}\right) + \hat{e} \sin\left(\frac{\theta}{2}\right) \quad (2.16)$$

and perform quaternion products in order to obtain the rotations.

By defining two quaternions as $p = \cos\left(\frac{\alpha}{2}\right) + \hat{e} \sin\left(\frac{\alpha}{2}\right)$ and $q = \cos\left(\frac{\beta}{2}\right) + \hat{e} \sin\left(\frac{\beta}{2}\right)$ we obtain the quaternion product as follows.

$$r = p \otimes q = \left(\cos\left(\frac{\alpha}{2}\right) + \hat{e} \sin\left(\frac{\alpha}{2}\right) \right) \otimes \left(\cos\left(\frac{\beta}{2}\right) + \hat{e} \sin\left(\frac{\beta}{2}\right) \right) \quad (2.17)$$

$$r = \cos\left(\frac{\alpha + \beta}{2}\right) + \hat{e} \sin\left(\frac{\alpha + \beta}{2}\right) = \cos(\gamma) + \hat{e} \sin(\gamma) \quad (2.18)$$

The product of two quaternions as seen above represents the two consecutive rotations by α and β . Equation 2.19 represents the rotation of a quaternion and a vector v

$$q \otimes v = (q_0 + q_v) \otimes (0 + v) = -q_v \cdot + q_0 v + q \times v \quad (2.19)$$

However, multiplying this expression by the conjugate of the quaternion q^* gives the expression in Equation 2.20 which is a vector and expressed further in the form of direction cosine matrix in Equation 2.21

$$w = q \otimes v \otimes q^* = \left(\cos^2\left(\frac{\alpha}{2}\right) - \sin^2\left(\frac{\alpha}{2}\right) \right) v + 2(q_v \cdot v)q_v + 2q_0(q_v \times v) \quad (2.20)$$

$$\begin{bmatrix} w_1 \\ w_2 \\ w_3 \end{bmatrix} = \begin{bmatrix} 2q_0^2 - 1 + 2q_1^2 & 2q_1q_2 - 2q_0q_3 & 2q_1q_3 + 2q_0q_2 \\ 2q_1q_2 + 2q_0q_3 & 2q_2^2 - 1 + 2q_0^2 & 2q_2q_3 - 2q_0q_1 \\ 2q_1q_3 - 2q_0q_2 & 2q_2q_3 - 2q_0q_1 & 2q_3^2 - 1 + 2q_0^2 \end{bmatrix} \begin{bmatrix} v_1 \\ v_2 \\ v_3 \end{bmatrix} \quad (2.21)$$

the DCM above can also be defined as a general rotational matrix

$$C = (2q_0^2 - 1)v + 2(q \cdot v)q + 2q_0(q \times v) \quad (2.22)$$

2.3.5 Error Quaternion

The error quaternion is defined as the rotational quaternion between two rotations. The error quaternion is obtained by quaternion product of the inverse quaternion

representing the desired quaternion of one point to another and the initial quaternion itself, given below

$$q_e = q^{-1}_d \otimes q \quad (2.23)$$

$$q_e = \begin{bmatrix} q_{d0} & q_{d1} & -q_{d2} & -q_{d3} \\ -q_{d1} & q_{d0} & q_{d3} & -q_{d2} \\ q_{d2} & -q_{d3} & q_{d0} & -q_{d1} \\ q_{d3} & q_{d2} & q_{d1} & q_{d0} \end{bmatrix} \begin{bmatrix} q_0 \\ q_1 \\ q_2 \\ q_3 \end{bmatrix} \quad (2.24)$$

The quaternion error q_e satisfies the unit quaternion constraint.

2.4 Sensors

The sensors used in the ADCS of ESTCube-2 include gyroscopic sensors, accelerometers, magnetometers, Sun sensors, and star tracker [19]. These were selected in order to be able to meet the pointing requirements and accurately obtain the attitude beyond LEO.

2.4.1 Gyroscopes

The satellite will consist of 4 gyroscopic sensors which have been selected and tested on a prototype sensor board.

2.4.2 Accelerometers

Two accelerometers will be used on the satellite mainly for closed loop control of the cold gas thrusters.

2.4.3 Magnetometers

The satellite will contain two Magnetometers which will be used mainly for attitude determination in LEO.

2.4.4 Sun sensor

On board the satellite will be 6 sun sensors which are developed in house. Though the sun sensors provide less accuracy than star tracker, they are required for more frequent measurements.

2.4.5 Star tracker

The star tracker is a separate subsystem and will be used to obtain very accurate and precise attitude information in combination with other sensors even during the satellite spin up.

2.5 Actuators

2.5.1 Reaction Wheels

Reaction wheels are actuators that provide fine attitude control which results from the acceleration of the flywheel. The rotational acceleration is as a result of an electric motor which could output a varied rotation. The control Torque produced is opposite to the rate of change of angular momentum of the wheel as given in the Equation.

$$T_c = -J \cdot \dot{\omega} = -\dot{H} \quad (2.25)$$

where

- T_c is control torque generated.

- J is the moment of inertia.
- w is the angular velocity vector.
- H is the angular momentum of the wheel.

The reaction wheels cannot be used exclusively as there is a build up in angular momentum of the wheels which makes it saturated. As such, the ACS also makes use of the thrusters and magnetic coils which will be used to generate external torque to unsaturate the angular momentum in the wheels. The reaction wheels used on ESTCube-2 has a momentum storage of $1.5mNms$.

2.5.2 Magnetic Coils

The magnetic coils or magnetic torquers or magnetorquers are wired coils used on the satellite that interacts with the Earth's magnetic field. The coils generate a strong magnetic dipole by passing current through the coils. The torque used for attitude control is proportional to the dipole moment of the torquer and strength of the Earth's magnetic field and thus depends on the angle between the two [20]. The torque reaction is also modeled based on the magnetic field and the current supplied to the coils as given in Equation 2.26

$$T_c = nIA(\hat{e} \times B) \quad (2.26)$$

where

- T_c is control torque generated.
- n is the number of turns on the coil.
- A is the cross sectional area of the coil.
- I is the current supplied through the coils.
- \hat{e} is the unit vector in the direction of the coil's axis.

The magnetorquers for ESTCube-2 are a similar design to those of ESTCube-1 [17]. For ESTCube-2, the area of the magnetorquers were increased based on the size of the 3U satellite and the demand for a larger magnetic torque. The magnetic moment of the magnetorquer is 0.5 A/m^2 in the three axis.

2.5.3 Cold Gas Thruster

Thrusters are mostly used in spacecraft in higher altitudes outside the significant influence of the Earth's magnetic field. They are needed for large attitude maneuvers. The thruster to be used on ESTCube-2 is the cold gas thruster developed by Nanospace AB and includes four thrust nozzles in the same -z axis direction. The nominal thrust is 1mN and the torque created is a product of the thrust and the distance to the centre of mass. More description on application of pulse width modulation on thrusters with control laws is given in [21].

3 Spacecraft Modeling

In this Chapter, I will describe the satellite dynamics with mathematical models and disturbances with view of obtaining an approximate linearized model for the satellite for controller implementation.

3.1 Kepler And Newton's Laws

The motion of celestial bodies have been studied and laws postulated by Johannes Kepler based on works of Tycho Brahe [22] [21]. With respect to orbital evaluation of two point masses, a model for a spacecraft orbiting a planet can be obtained be considering equations of motions and Newton's second law. Kepler postulated the following laws which apply to satellite motion in Earth's orbit

- *The orbit of each planet is an ellipse, with the Sun at one focus.*
- *The radius vector drawn from the planet to the Sun sweeps out equal areas in equal times.*
- *The square of the period of a planet is proportional to the cube of its mean distance from the Sun.*

These laws corresponds and also applies to spacecraft motion in Earth orbit, where the Sun represents the Earth and the planet represent the spacecraft in orbit.

3.2 Inertia Matrix

Based on the idea of inertia and due to the governing laws of dynamics, any force applied to a body other than from its center of mass will cause an intent to rotate. The rate of change of angular velocity of a body is proportional to the body's concentration of mass. Thus, a relationship between a body's momentum and rotation in inertia space can be defined as:

$$h = J\omega \quad (3.1)$$

The inertia matrix J can be obtained by relating the location of a portion of mass from the center of a body, r , and its rotational velocity as in equation 3.2

$$h = \int r \times (\omega \times r) dm \quad (3.2)$$

Thus the inertia matrix J about an arbitrary origin which is obtained by taking cross products of individual elements is defined by

$$J = \begin{bmatrix} J_x & -J_{xy} & -J_{xz} \\ -J_{yx} & J_y & -J_{yz} \\ -J_{zx} & -J_{zy} & J_z \end{bmatrix} \quad (3.3)$$

$$J = \begin{bmatrix} \int_v (y^2 + z^2) \rho_m dv & -\int_v (xy) \rho_m dv & -\int_v (xz) \rho_m dv \\ -\int_v (yx) \rho_m dv & \int_v (x^2 + z^2) \rho_m dv & -\int_v (yz) \rho_m dv \\ -\int_v (xz) \rho_m dv & -\int_v (zy) \rho_m dv & \int_v (x^2 + y^2) \rho_m dv \end{bmatrix} \quad (3.4)$$

where

- ρ_m is the density of the satellite
- v is represented as the volume

and J_x , J_y and J_z are the moments of inertia about the x, y and z axis respectively, and $J_{xy} = J_{yx}$, $J_{xz} = J_{zx}$ and $J_{yz} = J_{zy}$ are the products of inertia.

If the principal axes of inertia coincide with the axes of the body frame by being symmetric with its axes $J_{xy} = J_{xz} = J_{yz} = 0$, the inertia matrix reduces to:

$$J = \begin{bmatrix} J_x & 0 & 0 \\ 0 & J_y & 0 \\ 0 & 0 & J_z \end{bmatrix} \quad (3.5)$$

3.3 Environmental Models

This section will discuss and examine the environmental torque models. Spacecraft in orbit are subjected to a variety of environmental torques which affect its attitude. These could be either internal disturbance torques caused by the spacecraft or external environmental disturbances. The main disturbances to be evaluated will be magnetic disturbance torque, solar radiation pressure torque, aerodynamic torque and gravity-gradient torque and how much of influence they will have on ESTCube-2 considering the satellite in LEO and GEO. A disturbance torque based on the thruster axis misalignment will also be discussed and evaluated based on some values of misalignment.

3.3.1 Earth's Geomagnetic Field

Spacecrafts in LEO are greatly influenced by Earth's magnetic field. Hence application of magnetic control laws is dependent on the Earth's magnetic field. The geomagnetic field is extensively described in [23], a brief description of its model and effect on spacecraft is discussed here. The geomagnetic field can be modeled as a magnetic dipole which is tilted about 11.5 deg with the magnetic south near the geographical north pole and the magnetic north, near the geographical south pole as seen in Figure 3.1.

The geomagnetic field is much higher at altitudes closer to the Earth and decrease with an increase in altitude. The magnetic field strength at the equator is approximately 0.03mT [2] and as seen in Figure 3.1, lines are closer at the poles hence a

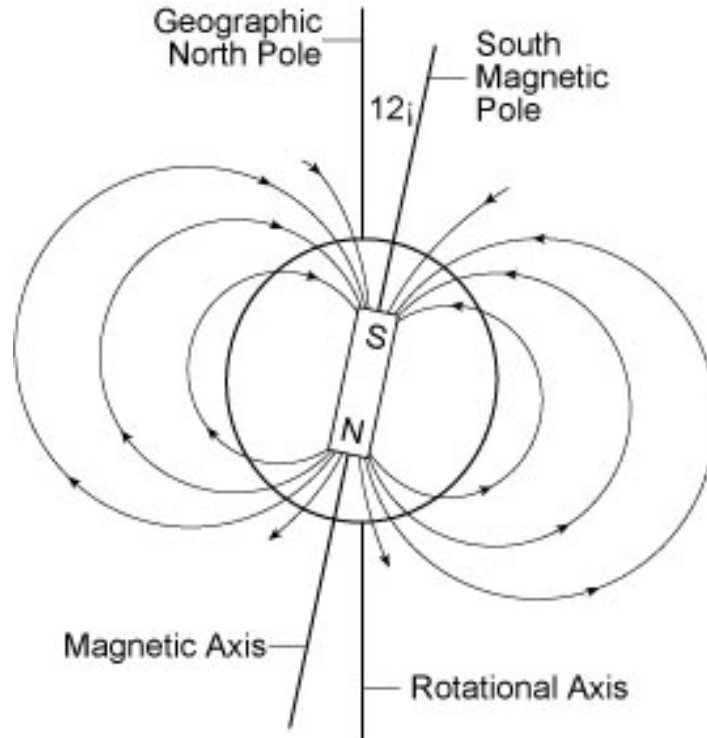


FIGURE 3.1: Earth's Magnetic Dipole [2].

stronger magnetic force experienced at the poles approximately twice the strength to that at the equator.

The International Geomagnetic Reference Field (IGRF) is a standard geomagnetic model used to describe the Earth's magnetic field. The IGRF models entails a lot of computation, however estimates of the Earth's magnetic field are done using a dipole model. Controllers are also designed based on the dipole model as effective designs can be made with regards errors in magnetic field measurements. The dipole model which will be used later in this work in the design of linear quadratic regulator is mathematically defined as [24]

$$b = \begin{bmatrix} b_1(t) \\ b_2(t) \\ b_3(t) \end{bmatrix} = \frac{\mu_f}{a^3} \begin{bmatrix} \cos \omega_0 t \sin \theta \\ -\cos \theta \\ 2 \sin \omega_0 t \sin \theta \end{bmatrix} \quad (3.6)$$

where θ is the inclination with respect to the geomagnetic equator, a is the orbit's semi major axis, ω_0 is the orbit angular velocity and μ_f is the magnetic field's

dipole strength in $Wb \cdot m$.

3.3.2 Gravity-Gradient Torque

Gravity-gradient disturbance is a torque felt by an Earth orbiting satellite due to the gravitational force between the earth and the satellite. The Earth's non-uniform gravitational field which according to Newton is inversely proportional to the square of the distance to the Earth causes this torque and also causes the satellite to obey Kepler's law of planetary motion as described in 3.1 The gravity-gradient torque on a body is derived as

$$T_g = \frac{3\mu}{2R_s^3} |\hat{R}_s \times (J \cdot \hat{R}_s)| \quad (3.7)$$

where

- μ is the gravitational constant of the earth.
- R_s is a vector representing the distance from the center of the earth to the satellite.
- J is the moment of inertia tensor of the satellite as described in 3.2.

Equation 3.7 could be used to obtain a detail analysis and also obtain the torques about each axis when the body frame is along the reference frame. However a more simplified equation is presented in [25] is used in this report based on the maximum gravity gradient disturbance torque.

$$T_g = \frac{3\mu}{2R_s^3} |J_z - J_y| \sin(2\theta) \quad (3.8)$$

where T_g is the maximum gravity torque, J_z and J_y are the largest and smallest moment of inertia, and θ is the maximum deviation from the local vertical.

Based on the formula given in 3.2 and a satellite mass of about $4kg$, the moments of inertia about the x, y and z axes are calculated to be $0.0333kg.m^2$, $0.0333kg.m^2$ and $0.0067kg.m^2$ respectively.

The gravity gradient torque can thus be calculated by applying a minimal deviation of 1 degree:

$$T_g = \frac{(3)(3.986 \times 10^{14})}{(2)(7078 \times 10^3)^3} |0.0067 - 0.033| \sin(2) \quad (3.9)$$

$$T_g = 1.547 \times 10^{-9} Nm$$

The torque value was obtained based on a 700km altitude orbit and from the equation notice that with an increase in the altitude orbit towards the lunar orbit, the value of this torque will continue to reduce and become quite insignificant. With a maximum deviation of 30 degrees, the torque obtained was $2.2 \times 10^{-8} Nm$

3.3.3 Aerodynamic Torque

Spacecrafts in LEO experience an interaction between the satellite surface and residual atmosphere. This results in the the aerodynamic torque which is quite a dominant disturbance torque for satellites lower altitudes. The disturbance torque can be modeled and describes as

$$T_{aero} = (r_{cp} - r_{cg}) F \quad (3.10)$$

where r_{cp} is the centre of pressure vector and r_{cg} is the centre of gravity vector. F is the atmospheric force which acts on the satellite and is described as

$$F = \frac{1}{2} \rho C_d A V^2 \quad (3.11)$$

where ρ is the atmospheric density, C_d is the atmospheric drag coefficient (usually used as 2), A is the satellite surface area and V is the spacecraft velocity. The torque always acts in the direction opposite to the satellite motion.

3.3.4 Solar Radiation Torque

The solar photons which impact on the surface of the satellite creates a force which produces a torque about the centre of mass of the satellite. The force acting on the satellite depends on if the incident radiation is absorbed or reflected. The torque is independent of the altitude of the satellite. The solar radiation torque is modeled as

$$T_s = (r_{cp} - r_{cg})F \quad (3.12)$$

where F is

$$F = \frac{F_s}{c}A(1 + q) \cos i$$

F_s is the solar constant ($1371W/m^2$), c is the speed of light ($3 \times 10^8m/s$), A is the surface area, q is the reflectant coefficient ranging between 0 and 1, i is the angle of incidence of the sun.

3.3.5 Residual Magnetic Torque

As experienced by satellites in LEO as well as in ESTCube-1 [26], a magnetic field is created in the satellite. While the satellite being controlled by the magnetic coils interacts with Earth's magnetic field, a magnetic field in the satellite is created by electric components and other ferromagnetic materials. This magnetic field is considered as a disturbance as it has an effect on the control of the satellite's attitude. The strength of this magnetic field and its direction cannot be easily determined before launch of the satellite, however measuring and calculating this residual magnetic torque is needed in other to augment for the disturbance in the design of the magnetic control laws. The residual magnetic torque can also be expressed the same way as the magnetorquers described in Section 2.5.2

$$\tau_{res} = m_{res} \times B \quad (3.13)$$

In ESTCube-1, the residual magnetic moment was the dominant disturbance torque in the satellite and it was estimated as $0.1Am^2$ [27]

3.4 Dynamics

As mentioned earlier, the quaternion based model has advantages in space technology applications over the Euler angle representations. The spacecraft dynamics model has been derived in several texts and here it is reviewed and simplified. In order to derive the dynamic model of the satellite, the satellite is assumed to act as a rigid body as well as a point mass in orbit. Hence Newton-Euler formulation is used where the angular momentum relates to the applied torque.

By application of Newton's second law to the spacecraft's rotational motion

$$M = \dot{h}_i \quad (3.14)$$

where

- h is the angular momentum
- M is the applied torque or external moment in inertial frame with reference to body frame

in view of coriolis equation [28], (3.14) can be expressed as

$$M = \dot{h} + \omega_i \times h \quad (3.15)$$

therefore, the rate of angular momentum can be defined as

$$\dot{h} = J\dot{\omega}_i = -\omega_i \times J\omega_i + M \quad (3.16)$$

M can be expressed as addition of all disturbance torques and a control torque T_c

$$J\dot{\omega}_i = T_d + T_c - \Omega(\omega_i)J\omega_i \quad (3.17)$$

where

- $\Omega(\omega_i)$ is the skew symmetric representation of the angular velocity in inertial reference frame.

$$\Omega(\omega_i) = \begin{bmatrix} 0 & -\omega_1 & -\omega_2 & -\omega_3 \\ \omega_1 & 0 & \omega_3 & -\omega_2 \\ \omega_2 & -\omega_3 & 0 & \omega_1 \\ \omega_3 & \omega_2 & -\omega_1 & 0 \end{bmatrix} \quad (3.18)$$

- T_d is the sum of disturbance torques acting on the satellite
- T_c is the applied control input torque

The varying torques acting on the satellite changes with respect to the selection of actuator for specific attitude operation.

3.5 Kinematics

The kinematic model describes the orientation of the satellite by integrating the angular velocity. The kinematic differential equations represented in quaternions as derived in [23]

$$\dot{q} = -\frac{1}{2}\omega \times q_v + \frac{1}{2}q_o\omega \quad (3.19)$$

$$\dot{q}_0 = -\frac{1}{2}\omega^T q_v \quad (3.20)$$

The quaternion representation that rotates body frame in relation with the reference frame is

$$q = [q_o, q_v^T]^T = \left[\cos\left(\frac{\alpha}{2}\right), \hat{e}^T \sin\left(\frac{\alpha}{2}\right) \right]^T \quad (3.21)$$

where we define the rotational axis by a unit vector \hat{e} and the angle of rotation around that axis by α . The vector q_e described by $\hat{e}^T \sin\left(\frac{\alpha}{2}\right) = [q_1, q_2, q_3]^T$ and the

scalar component of the quaternion by $q_0 = \cos(\frac{\alpha}{2})$. Thus from (3.19), we obtain

$$\begin{bmatrix} \dot{q}_0 \\ \dot{q}_1 \\ \dot{q}_2 \\ \dot{q}_3 \end{bmatrix} = \frac{1}{2} \begin{bmatrix} 0 & -\omega_1 & -\omega_2 & -\omega_3 \\ \omega_1 & 0 & \omega_3 & -\omega_2 \\ \omega_2 & -\omega_3 & 0 & \omega_1 \\ \omega_3 & \omega_2 & -\omega_1 & 0 \end{bmatrix} \begin{bmatrix} q_0 \\ q_1 \\ q_2 \\ q_3 \end{bmatrix} = \frac{1}{2} \begin{bmatrix} q_0 & -q_1 & -q_2 & -q_3 \\ q_1 & q_0 & -q_3 & q_2 \\ q_2 & q_3 & q_0 & -q_1 \\ q_3 & -q_2 & q_1 & q_0 \end{bmatrix} \begin{bmatrix} 0 \\ \omega_1 \\ \omega_2 \\ \omega_3 \end{bmatrix} \quad (3.22)$$

The vector component can be easily obtained from the property of quaternion given in section 2.3 $q_0 = \sqrt{1 - q_1^2 - q_2^2 - q_3^2}$

$$\begin{bmatrix} \dot{q}_1 \\ \dot{q}_2 \\ \dot{q}_3 \end{bmatrix} = \frac{1}{2} \begin{bmatrix} q_0 & -q_3 & q_2 \\ q_3 & q_0 & -q_1 \\ -q_2 & q_1 & q_0 \end{bmatrix} \begin{bmatrix} \omega_1 \\ \omega_2 \\ \omega_3 \end{bmatrix} \quad (3.23)$$

3.6 Linearization

The satellite model equations as given in 3.17 and 3.23 represents the non linear dynamics and kinematics models. In order to use these equations for an optimal controller such as the Linear Quadratic Controller, these nonlinear equations have to be linearized.

The linear form of the satellite attitude equations can be obtained by linearizing the equations about an equilibrium or stationary point. The linearization points based on a first order Taylor expansion about the stationary point are selected and given as in 3.24

$$q = \begin{bmatrix} 1, 0 \end{bmatrix}^T \quad (3.24)$$

Equation 3.23 can be represented as a function

$$\dot{q}_v = g(q, \omega_i) \quad (3.25)$$

therefore a partial derivative will be represented as

$$\dot{q}_v = \frac{\partial g}{\partial q}(q) + \frac{\partial g}{\partial \omega_i}(\omega_i) \quad (3.26)$$

linearizing with change around the equilibrium point e , assume at equilibrium we have stationary point where $q_1 = q_2 = q_3 = 0$ and $\omega_i = 0$.

$$\dot{q}_v - \dot{q}_e = \frac{\partial g}{\partial q}(q - q_e) + \frac{\partial g}{\partial \omega_i}(\omega_i - \omega_{ie}) \quad (3.27)$$

expanding equation 3.23 yields the following equations

$$\dot{q}_1 = \frac{1}{2}(q_0\omega_1 - q_3\omega_2 + q_2\omega_3) \quad (3.28)$$

$$\dot{q}_2 = \frac{1}{2}(q_3\omega_1 + q_0\omega_2 - q_1\omega_3) \quad (3.29)$$

$$\dot{q}_3 = \frac{1}{2}(-q_2\omega_1 + q_1\omega_2 + q_0\omega_3) \quad (3.30)$$

with respect to equation 3.27, the above equations 3.28, 3.29 and 3.30 becomes

$$\dot{q}_1 = 0 - 0 + 0 + \frac{1}{2}(q_0) - 0 + 0 \quad (3.31)$$

$$\dot{q}_2 = 0 + 0 - 0 + 0 + \frac{1}{2}(q_0) + 0 \quad (3.32)$$

$$\dot{q}_3 = -0 + 0 + 0 - 0 + 0 + \frac{1}{2}(q_0) \quad (3.33)$$

Therefore the matrix representation is expressed as

$$\begin{bmatrix} \dot{q}_1 \\ \dot{q}_2 \\ \dot{q}_3 \end{bmatrix} = \begin{bmatrix} 0 & 0 & 0 & \frac{1}{2}(q_0) & 0 & 0 \\ 0 & 0 & 0 & 0 & \frac{1}{2}(q_0) & 0 \\ 0 & 0 & 0 & 0 & 0 & \frac{1}{2}(q_0) \end{bmatrix} \begin{bmatrix} q_1 \\ q_2 \\ q_3 \\ \omega_1 \\ \omega_2 \\ \omega_3 \end{bmatrix} \quad (3.34)$$

$$\dot{q}_v = \begin{bmatrix} 0_3 & \frac{1}{2}(I_3) \end{bmatrix} \begin{bmatrix} q_v \\ \omega_i \end{bmatrix} \quad (3.35)$$

where $q_0 = 1$ at equilibrium.

Also by performing the expansion and linearization of 3.17 and assuming the approximation with negligible disturbance torque.

$$J\dot{\omega}_i \approx T_c \quad (3.36)$$

$$\begin{bmatrix} \dot{q}_v \\ \dot{\omega}_i \end{bmatrix} = \begin{bmatrix} 0_3 & \frac{1}{2}(I_3) \\ 0_3 & 0_3 \end{bmatrix} \begin{bmatrix} q_v \\ \omega_i \end{bmatrix} + \begin{bmatrix} 0_3 \\ J^{-1} \end{bmatrix} (T_c) \quad (3.37)$$

$$= Ax + Bu \quad (3.38)$$

where u represents the control input T_c and

$$A = \begin{bmatrix} 0_3 & \frac{1}{2}(I_3) \\ 0_3 & 0_3 \end{bmatrix}, x = \begin{bmatrix} q_v \\ \omega_i \end{bmatrix}, B = \begin{bmatrix} 0_3 \\ J^{-1} \end{bmatrix} \quad (3.39)$$

4 Attitude Control for ESTCube-2

4.1 Description and Control Specifications for ESTCube-2

Based on the mission objectives for ESTCube-2, the centrifugal deployment of E-sail Tether requires enough angular momentum, as such the control design should spin up the satellite to one revolution per second (360 deg/s). For this purpose, the satellite spin axis must be aligned with the Earth's polar axis with pointing error of less than 3 degrees [27]. Also for ground station pointing and Earth observation, the pointing accuracy should be less than 0.1 degrees.

4.2 Detumbling Controller Designs

The purpose of the detumbling mode is to detumble or stabilize the angular rate of the satellite after orbital insertion or release from the launch vehicle and to ensure that the satellite can be in a controllable state. The controller designed for this mode must be able to regain control of the satellite in situations where control of the satellite has been lost. In general, the kinetic energy of the satellite is reduced, thus causing a reduction in the angular velocity of the satellite for optimal control.

The controller used in this mode is selected because the commanded magnetic dipole moment can be obtained directly from the calculations and is used as an input for the actuator. Also, the magnetometer measurement can always be read and used for the control algorithm

4.2.1 B-dot Controller Design

The B-dot controller had been specifically chosen for detumbling of the satellite. This is in view of the fact that it only requires the derivative of the magnetic field as input making it the best choice in terms of efficiency even when other orbital parameters could be missing.

The B-dot is derived by observing a decrease in the rotational energy during detumbling. This basically means that the scalar product of the angular velocity and the control torque must be negative

$$\omega_i^T \cdot \tau < 0 \quad (4.1)$$

where τ is represented as the control torque delivered by magnetic actuator and is expressed as

$$\tau = m \times B \quad (4.2)$$

where m is the commanded magnetic dipole moment and B is the geomagnetic field vector. A seemingly accurate model of the geomagnetic field for LEO circular orbit such as IGRF is being used as the model for the simulation.

the condition in equation 4.1 then becomes

$$\omega_i^T \cdot (m \times B) < 0 \quad (4.3)$$

Applying cross product rules given in section 2.3, the condition in 4.3 can be rewritten as

$$-m^T \cdot (\omega_i \times B) < 0 \quad (4.4)$$

In order to decrease the kinetic energy of the spacecraft the control torque τ has to be proportional to $-\omega$ and based on the above inequality, the magnetic moment needs to be perpendicular to $\omega \times B$ as no torque will be produced if it were parallel. We can therefore complete the solution by implementing a scalar gain k

$$m = -k \cdot (\omega_i \times B) \quad (4.5)$$

where k is a positive gain. The change in magnetic field vector is assumed to be mainly as a result of rotation of the satellite

$$\dot{B} \approx (\omega_i \times B) \quad (4.6)$$

therefore we can obtain a simple control law based on

$$m = -k\dot{B} \quad (4.7)$$

4.2.2 P Controller Designs

A P-controller could be implemented for detumbling of the satellite using reaction wheels. The proportional controller designed is based on the principle that the torque produced by the reaction wheel for the attitude control is opposite to the angular momentum change of the reaction wheel as described in section 2.5.1. This control law is simply the multiplication of the angular velocity of the satellite with a proportional gain.

$$T_c = k_\omega \omega_i \quad (4.8)$$

This control law may not be effective for detumbling at high angular velocity, but can be mainly used for nutation damping to implement nadir pointing as the

maximum torque generated with the reaction wheel is $0.0001Nm$ and hence will require unloading upon saturation of the reaction wheels.

4.2.3 PD Controller Designs

The PD controller designed is an implementation of the magnetic control law as defined in equation 4.2. The control law makes use of the magnetic field vector and the angular velocity and attitude of the satellite. The PD control implemented here is a simple controller model used for both magnetic coils and reaction wheels. While this control law attenuates the initial angular velocities, it also keeps the quaternion attitude at zero for all three axes. This control law makes use of calculated error vector to determine the most favourable magnetorquing moment for use with the magnet torquers. This is then utilized directly as the required torque vector. The error vector is composed of the quaternion error and the angular velocity in the body axes.

$$\vec{e} = k_{\omega}(\omega_i \times B) + k_q(q_e \times B) \quad (4.9)$$

where B is the magnetic field vector. K_{ω} and K_q are the controller gains which are chosen based on the performance of several tests of the system. q_e is the quaternion error defined as

$$q_e = \begin{bmatrix} q_{d0} & q_{d1} & -q_{d2} & -q_{d3} \\ -q_{d1} & q_{d0} & q_{d3} & -q_{d2} \\ q_{d2} & -q_{d3} & q_{d0} & -q_{d1} \\ q_{d3} & q_{d2} & q_{d1} & q_{d0} \end{bmatrix} \begin{bmatrix} q_0 \\ q_1 \\ q_2 \\ q_3 \end{bmatrix} \quad (4.10)$$

4.3 Pointing Controller Designs

The controllers designed for the pointing mode of the satellite is aimed to satisfy the requirements specified for pointing [29]. As such a simple PD controller for employed to both magnetic torquers and reaction wheels is described. Furthermore,

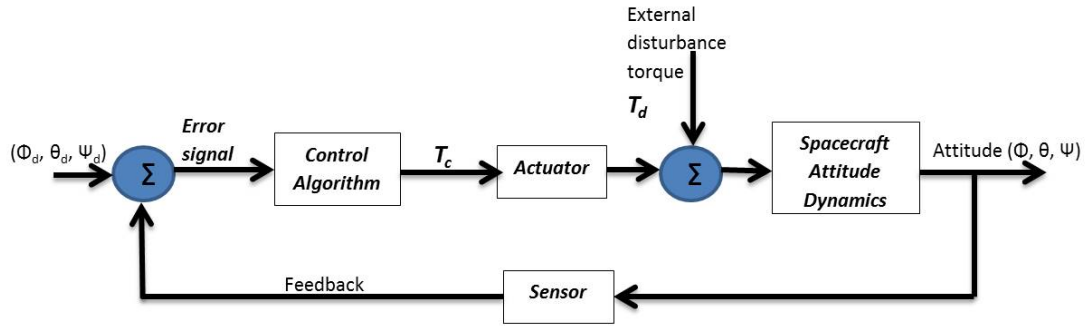


FIGURE 4.1: Attitude Control block diagram with feedback.

to ensure stability in precise pointing, a Linear Quadratic Regulator is designed based on a linearization of the satellite model for nadir pointing. Figure 4.4 shows a block diagram of a control algorithm which takes the error signal input and obtains a control torque to the actuator (reaction wheel) which attempts to rotate the spacecraft to the desired attitude.

4.3.1 PD Controller

For 3-axis pointing control, the PD controller structure described in Section 4.2.3 is implemented. The reaction wheels are applied to be able to provide quick angle maneuvers, however the limitation is in the maximum angular momentum that can be generated from the reaction wheel used prior to its saturation. The control law makes use of the quaternion error and feedback in 4.10. The control torque is generated as follows

$$\begin{bmatrix} T_{cx} \\ T_{cy} \\ T_{cz} \end{bmatrix} = \begin{bmatrix} k_{\omega}\omega_i + k_q q_e \end{bmatrix} \quad (4.11)$$

4.3.2 Linear Quadratic Regulator Design

The LQR control technique is designed here for the attitude stabilization during pointing. In order to satisfy strict requirements, the LQR is used in designing

linear controllers for such complex non linear systems like the CubeSat. The design aims to find a cost function and minimize this cost function.

$$\dot{x} = Ax + Bu \quad (4.12)$$

Based on the linearized satellite model designed for nadir pointing in [C](#) with state space quaternion model given in Equation [4.12](#), the controller implements a basic feedback control u for optimization,

$$u = -Kx \quad (4.13)$$

where K is the feedback gain matrix calculated to minimize the Linear Quadratic cost function

$$J = \int_0^{\infty} [x^T Qx + u^T Ru] dt \quad (4.14)$$

where Q and R are positive definite matrices known as the state weight matrix and control input weight matrix respectively, where Equation [4.13](#) is further expressed as

$$u = -R^{-1}B^T Px \quad (4.15)$$

where P is a symmetric positive semi-definite solution of the Algebraic Riccati Equation (ARE) given below

$$0 = PA + A^T P + Q - PBR^{-1}BP \quad (4.16)$$

Based on the calculated value for the gain K , $|A - BK|$ must be stable to obtain a correct and optimal result. For stability it can be analysed that the eigenvalues must have negative real parts. Hence Equation [4.16](#) is only solvable if and only if input matrices A and B is controllable. For controllability analysis see [Appendix A](#).

The designed LQR controller convergently stabilizes the nonlinear satellite model by attempting to bring the initial attitude and angular velocity to the minimal

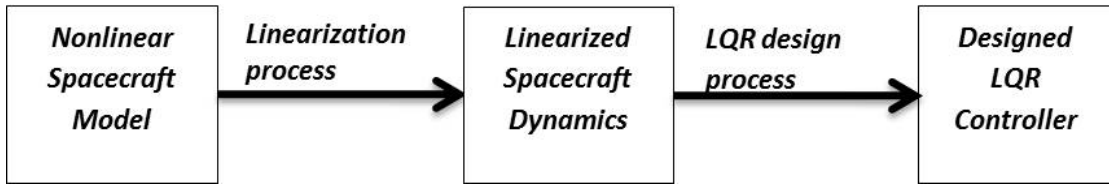


FIGURE 4.2: LQR design from linearization.

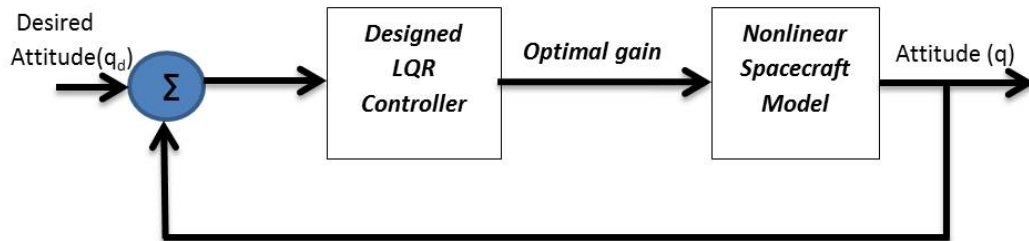


FIGURE 4.3: LQR controller on nonlinear spacecraft model.

equilibrium point. At this equilibrium point, the linearised model approximates the non linear model as efficiently as possible.

The satellite state x is given as

$$x = [q_{e1} \ q_{e2} \ q_{e3} \ \omega_1 \ \omega_2 \ \omega_3]^T \quad (4.17)$$

where q_{e1} q_{e2} q_{e3} can be defined as the quaternion error to obtain the desired attitude in quaternion for pointing which can be calculated from the quaternion error defined in 2.3.5.

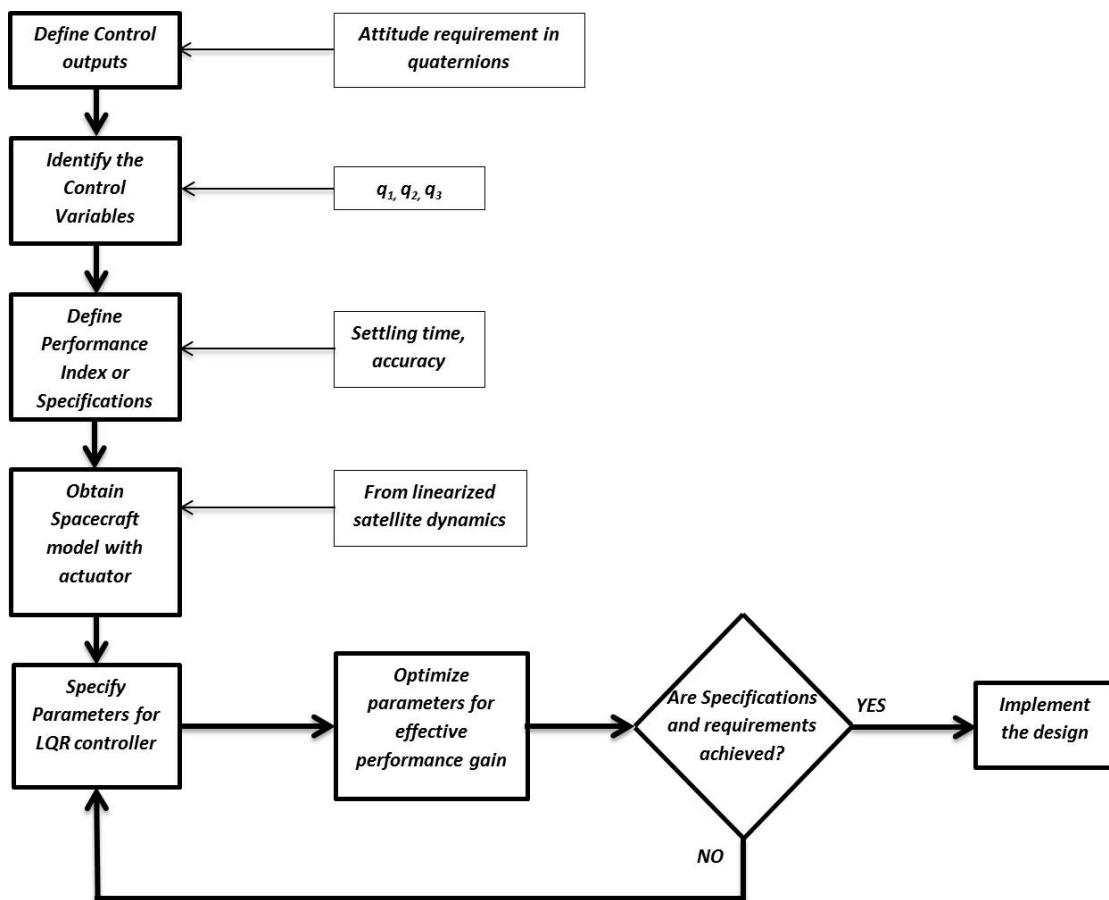


FIGURE 4.4: LQR controller design algorithm.

4.4 Cross Product Control Law

The controllability of the reaction wheels is limited by the saturation of the wheels unlike the magnetorquers which are subject to the geomagnetic field. To solve this, several approaches for wheel desaturation and unloading have been discussed and developed [5, 30–32]. Here a very simple cross product law is implemented to perform the pointing of the satellite by constantly. This control algorithm is based on the reaction wheel PD control law while constantly verifying the angular momentum of the wheel as a feedback. The magnetorquer is enabled in the algorithm when the angular momentum of the wheel approaches $1.5m.N.m.s$ as described in the Equations below

$$\begin{bmatrix} T_{cx} \\ T_{cy} \\ T_{cz} \end{bmatrix} = \begin{bmatrix} k_{\omega}\omega_i + k_q q_e \end{bmatrix} \quad (4.18)$$

$$m = -\frac{k}{(\|B\|)^2} [B \times h_e] \quad (4.19)$$

where T_c is the control torque from the reaction wheels, k, k_{ω}, k_q are gains for the algorithm, m is the magnetorquer dipole moment vector in SBRF and h_e is the angular momentum error of the wheels.

4.5 Spin-up Controller Designs

The spin up control algorithm designed will aim to spin the satellite to achieve an angular velocity of 360 deg/s . This high spin rate is based on mission requirement of spinning the satellite to generate enough angular momentum for the centrifugal deployment of tether for the plasma break experiment [19].

In order to control the spin motion of the satellite, three important control factors needs to be simultaneously considered. These are spin control, precession control, nutation control [33]. The spin rate controller designed here makes use of the

magnetorquers based on the strong magnetic field in the LEO environment. As the ESTCube-2 CubeSat would be used to test algorithms for the ESTCube-3 which is to be launched in Lunar orbit, a spin rate control based on reaction wheels and cold gas thrusters will also be designed but not covered in the scope of this thesis. The control law which is based on a Lyapunov like function satisfies the spin rate and nutation control while aligning the spin axis with Earth's polar axis. This is obtained by considering the rate of angular momentum as defined in Equation 3.17 to be

$$\dot{h} = T_c - \Omega(\omega_i)J\omega_i \quad (4.20)$$

Here we consider the disturbance torque to be negligible and the angular momentum error to be $h_e = h - h_d$, therefore the rate of angular momentum error is given as

$$\dot{h}_e = T_c - \Omega(\omega_i)h_e \quad (4.21)$$

Since we desire a spin about the x-axis, we define the angular momentum error $h_e = 0$, then $h_x = h_d$. We assume the principal axes of inertia coincide with the axes of the body frame, therefore Equation 3.5 holds and the angular rates in the transverse axes be controlled where $w_2 = w_3 = 0$. Then we assume $J_y = J_z = J_t$ and Equation 4.20 becomes

$$\begin{bmatrix} J_x \dot{\omega}_1 \\ J_t \dot{\omega}_2 \\ J_t \dot{\omega}_3 \end{bmatrix} = T_c - \begin{bmatrix} 0 & -\omega_3 & \omega_2 \\ \omega_3 & 0 & -\omega_1 \\ -\omega_2 & \omega_1 & 0 \end{bmatrix} \begin{bmatrix} J_x \omega_1 \\ J_t \omega_2 \\ J_t \omega_3 \end{bmatrix} \quad (4.22)$$

where J_t is the transverse component of the inertia matrix of the satellite and simplified further to

$$\begin{bmatrix} J_x \dot{\omega}_1 \\ J_t \dot{\omega}_2 \\ J_t \dot{\omega}_3 \end{bmatrix} = T_c + \begin{bmatrix} 0 \\ (J_t - J_x)(\omega_1 \omega_3) \\ (J_x - J_t)(\omega_1 \omega_2) \end{bmatrix} \quad (4.23)$$

Therefore the rate of angular momentum about the spin axis is given as

$$\dot{h}_1 = J_x \dot{\omega}_1 = T_c \begin{bmatrix} 1 & 0 & 0 \end{bmatrix} \quad (4.24)$$

and the error is then calculated to be $h_{e1} = h_1 - h_d$ and error rate therefore is

$$\dot{h}_{e1} = T_c \begin{bmatrix} 1 & 0 & 0 \end{bmatrix} \quad (4.25)$$

The control law is then defined based on the time derivative of a Lyapunov function V defined in [34]

$$\dot{V} = (h_e^T + k_1 h_{e1} \begin{bmatrix} 1 & 0 & 0 \end{bmatrix} + k_2 \omega^T P) T_c \quad (4.26)$$

and simplified further in the control equation given below for the required spin rate of the satellite in the x-axis for tether deployment.

$$m = -\frac{k}{(\|B\|)^2} [B \times (h_e + k_1 h_{e1} \begin{bmatrix} 1 \\ 0 \\ 0 \end{bmatrix} + k_2 S \omega)] \quad (4.27)$$

where m is the magnetorquer dipole moment vector in SBRF and k, k_1, k_2 are control law gains. S represents the axes selection matrix.

This control law and gains needs to be adjusted for the specific implementation of the tether deployment and ran in an iterative loop sequence. In obtaining preliminary results for the optimal performance of the controller, the following points are noted:

- The B-dot algorithm described Section 4.2.1 for detumbling of the satellite should first be used to reduce the angular momentum of the satellite in order to improve the performance of the spin up algorithm.
- For the iterative loop in running the controller, the initial desired angular velocity should be approximately 45 *deg/s* to ensure stability along the spin axis.

- The value of the control gains should be set as: $k_2 > 1$, $k_1 < 1$, $k \gg k_1$ to augment the nutation damping process and avoid uncontrolled spinning of the satellite about the transverse axis.

5 Simulation Results and Controller Comparison

This section presents results of the controllers designed and their performances to the system set with varying initial conditions. The attitude control system was designed and simulated with MATLAB and SIMULINK.

5.1 B-dot Controller Analysis

The results of the control algorithm described in Section 4.2.1 are depicted in Figures 5.1 to 5.3. The angular velocity components are seen to attain a steady state with zero error. As evident with magnetic control, the response has a fast transient and tends to converge at steady state with a very slow response. The response shown is based on setting the frequency to $100Hz$.

5.2 PD Controller Analysis

The PD controllers were tested with several cases while applying varying gains to determine an optimum performance. The performance overview is presented in Table 5.1 and result shown in Figures 5.4 to 5.14.

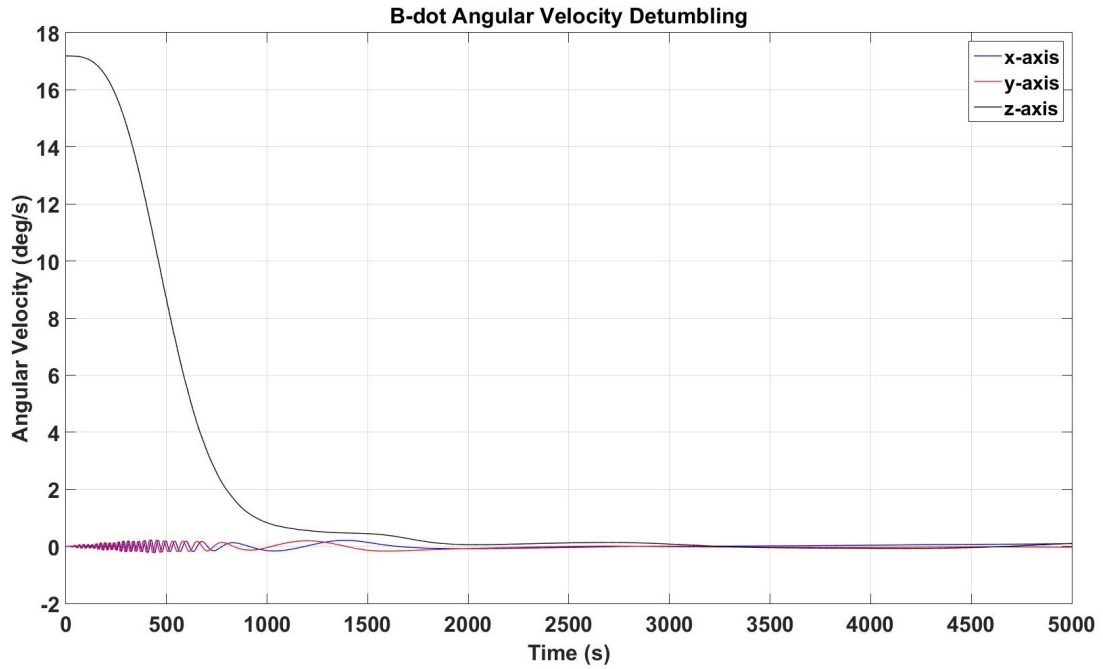


FIGURE 5.1: Detumbling of Satellite with Bdot Control

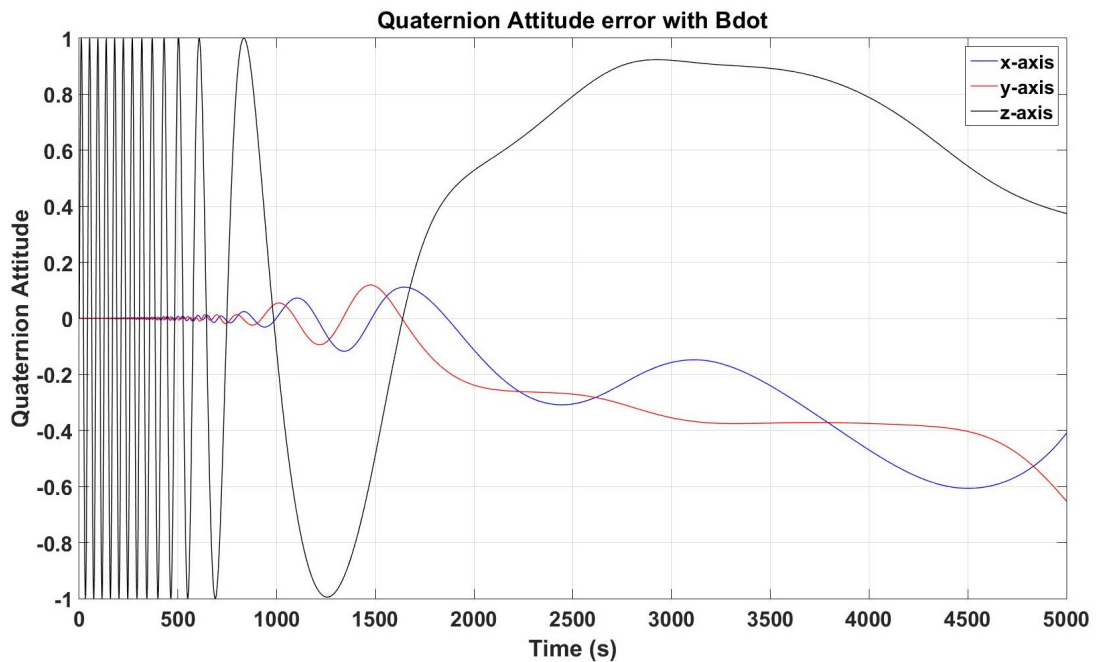


FIGURE 5.2: Quaternion Attitude during detumbling phase.

5.2.1 PD performance with Magnetorquers

The simulations with the magnetorquers were performed with an initial angular velocity of $(0.05, 0.05, 0.3) \text{ rad/s}$ and demonstrate in Figure 5.4 that the proposed control law achieves attenuating of the satellite angular velocity in approximately

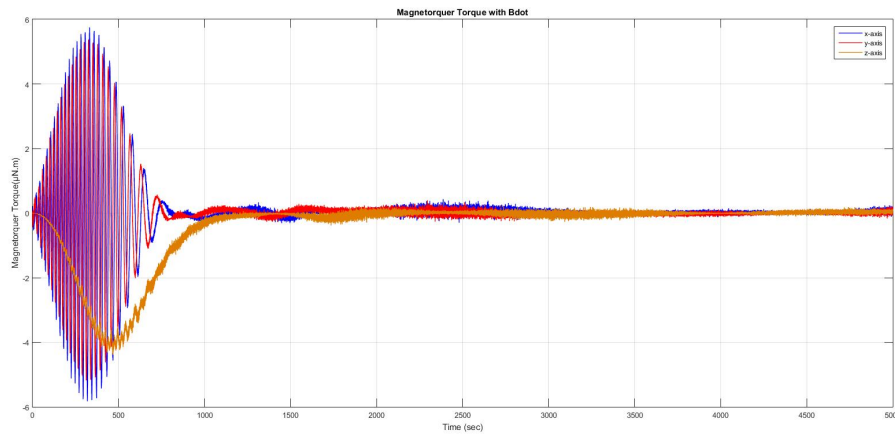


FIGURE 5.3: Magnetorquer Torque response during detumbling phase.

Parameters	Value	Unit
Orbit Period T_o	5400	Sec
Orbit Angular Velocity	$\omega_o = 2\pi/T_o$	Rads/sec
Parameters	Reaction Wheels	Magnetoquers
K_w	10^{-3}	100
K_q	10^{-2}	20000
Initial Angular Velocity	$(0.1, 0.1, 0.3)rad/s$	$(0.05, 0.05, 0.3)rad/s$
Initial Quaternion attitude	$(0, 0, 0, 1)$	$(0, 0, 0, 1)$

TABLE 5.1: PD Performance Overview.

1 orbit. Also the control law begins to maintain a stabilized attitude in approximately 9 orbits in all axes towards nadir pointing. The torque produced is seen to decline in about 1000secs as the oscillations of the angular velocity begins to attenuate.

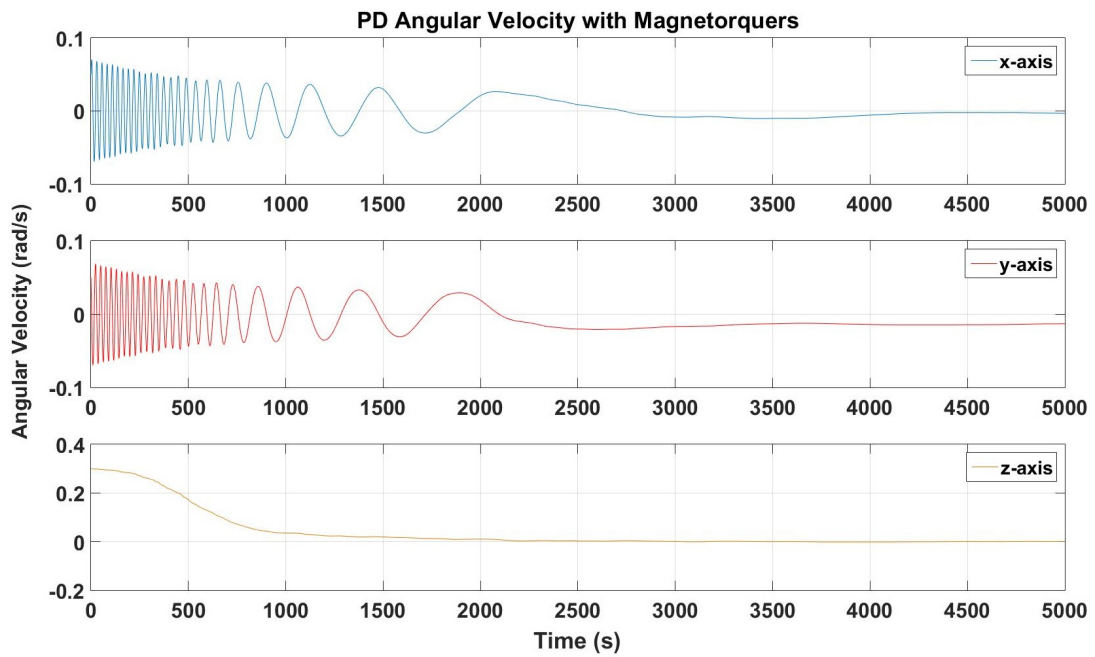


FIGURE 5.4: PD controller Angular velocity for Detumbling/Pointing with Magnetorquer.

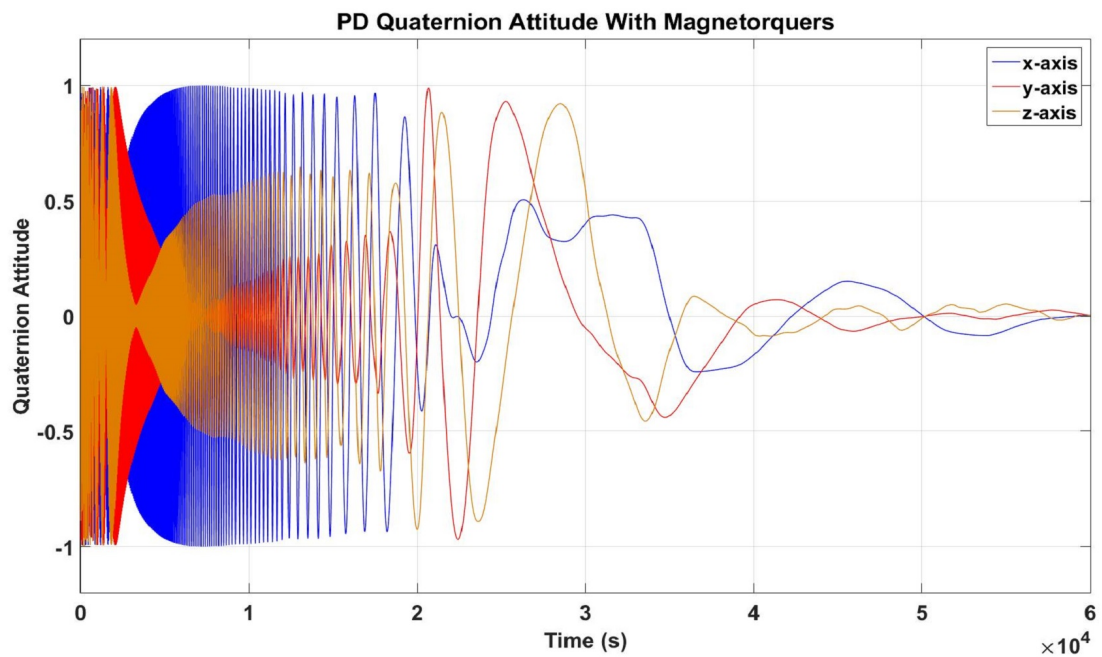


FIGURE 5.5: PD controller Quaternion Attitude for Detumbling/Pointing with Magnetorquer .

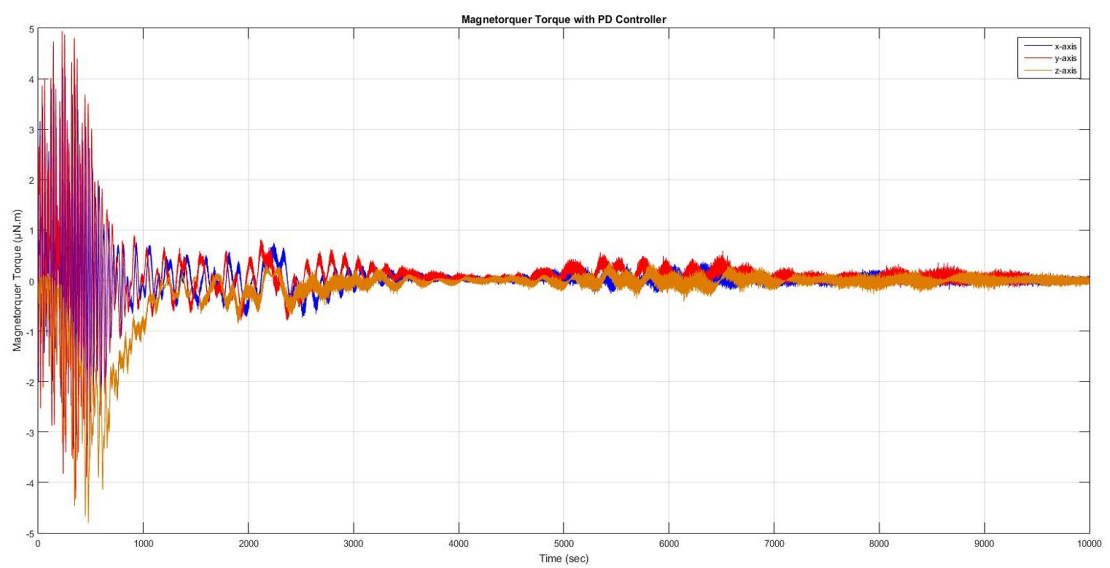


FIGURE 5.6: Magnetorquer Torque response.

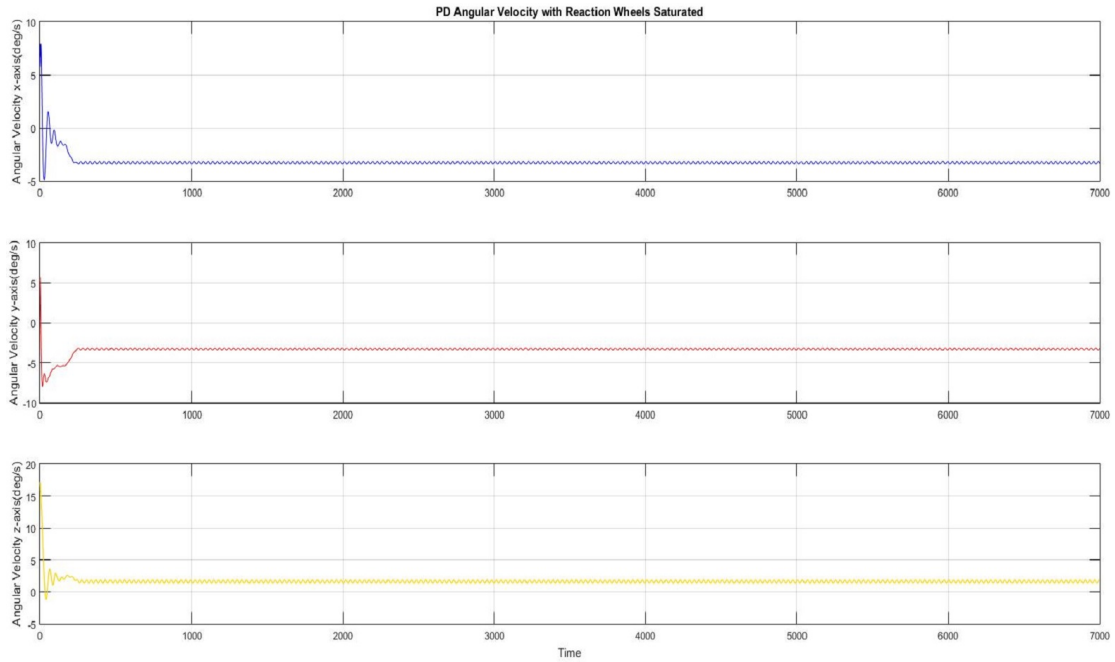


FIGURE 5.7: PD controller Angular velocity for Detumbling/Pointing with reaction wheels saturated

5.2.2 PD performance with saturated Reaction Wheels

The performance of the reaction wheel is hampered due to the saturation of the wheels as presented in Figure 5.7. The initial angular velocity was set at $(0.1, 0.1, 0.3)rad/s$, the reaction wheels were unable to successfully detumble the satellite to $(0, 0, 0)rad/s$. Also, the attitude of the satellite keeps oscillating on all axes. Figures 5.9 and 5.10 shows the angular momentum and torque of the reaction wheels respectively with the momentum maximizing at $0.0015N.m.s$ in approximately $250secs$ in all axes.

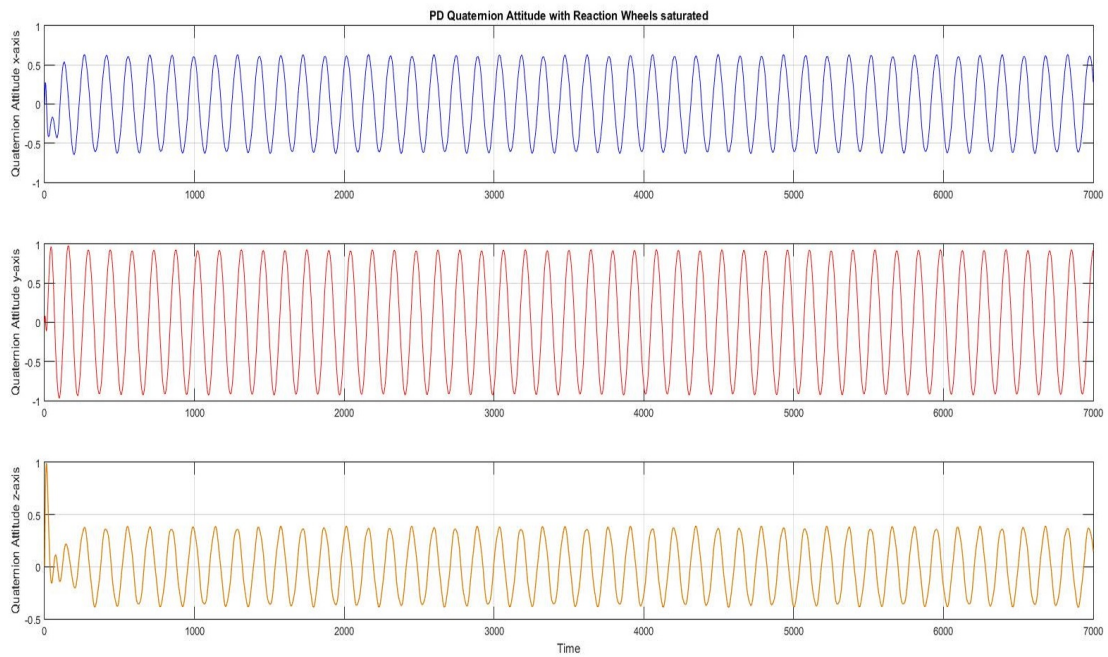


FIGURE 5.8: PD controller Quaternion Attitude for Detumbling/Pointing with reaction wheels saturated

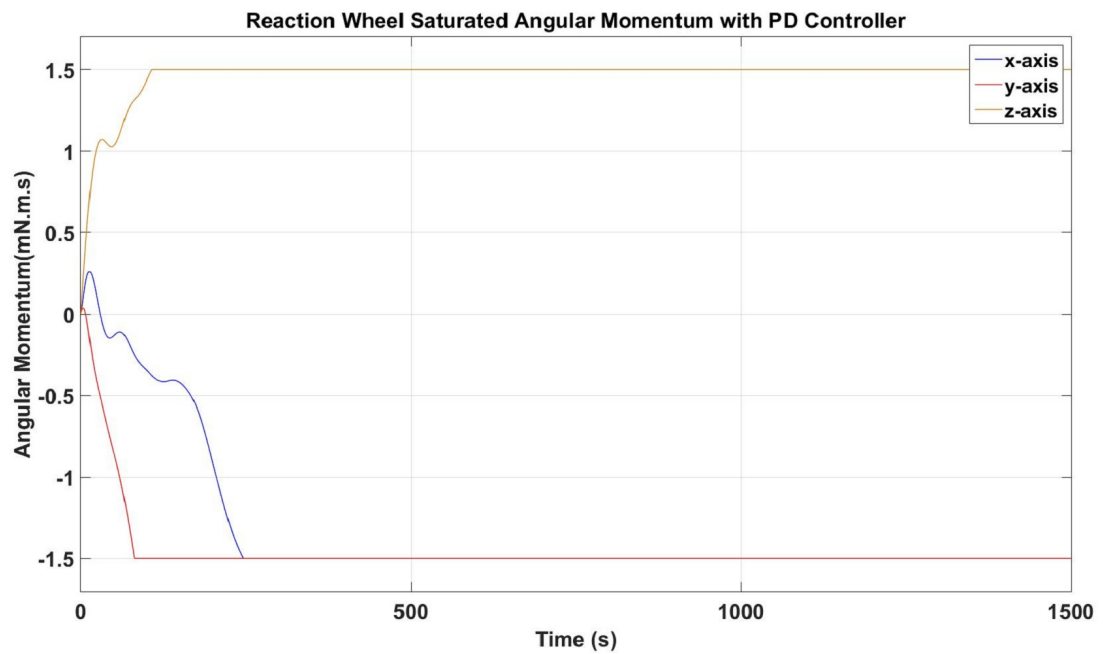


FIGURE 5.9: Angular momentum showing reaction wheels saturated

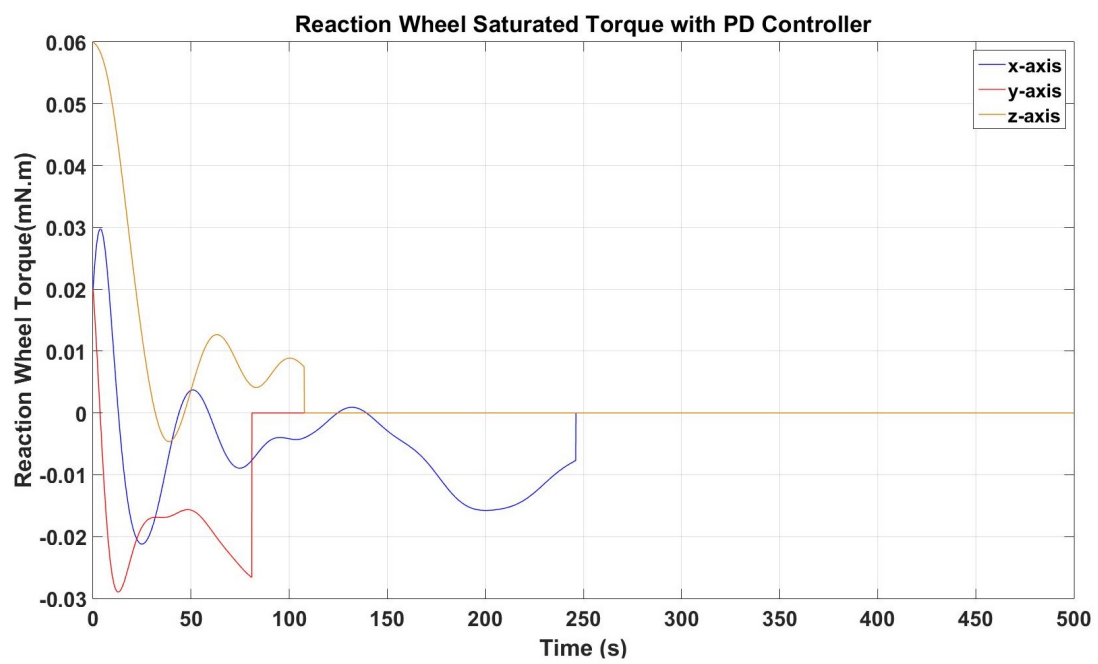


FIGURE 5.10: Reaction Wheel saturated torque response

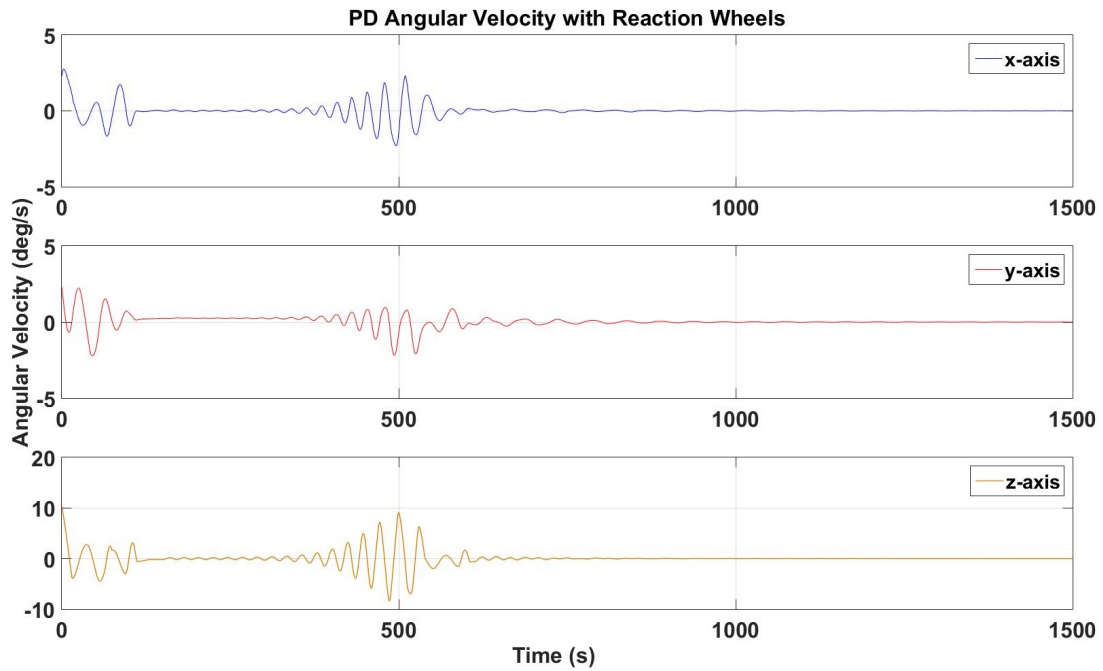


FIGURE 5.11: PD controller Angular velocity for Detumbling/Pointing with reaction wheels

5.2.3 PD performance with unsaturated wheels

The PD control law simulations were tested with the reaction wheels at an initial angular velocity lowered to $(0.04, 0.04, 0.18)rad/s$ and can be seen that the reaction wheel does not get saturated with this initial velocity. The satellite as seen in Figure 5.11 stabilizes to 0 deg in all axes in about 750secs and also maintains the desired nadir pointing mode in a similar time frame. The angular momentum and reaction wheel torque response are presented in Figures 5.13 and 5.14 with the angular momentum maintaining a value with magnitude less than $0.0015N.m.s$ in all axes.

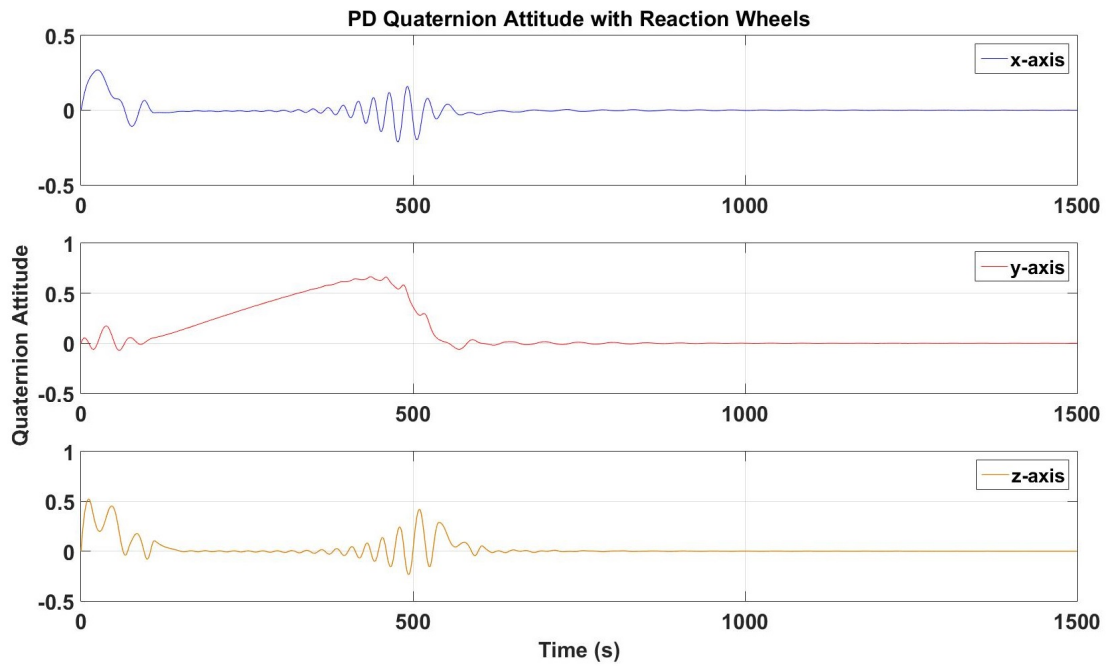


FIGURE 5.12: PD controller Quaternion Attitude for Detumbling/Pointing with reaction wheels

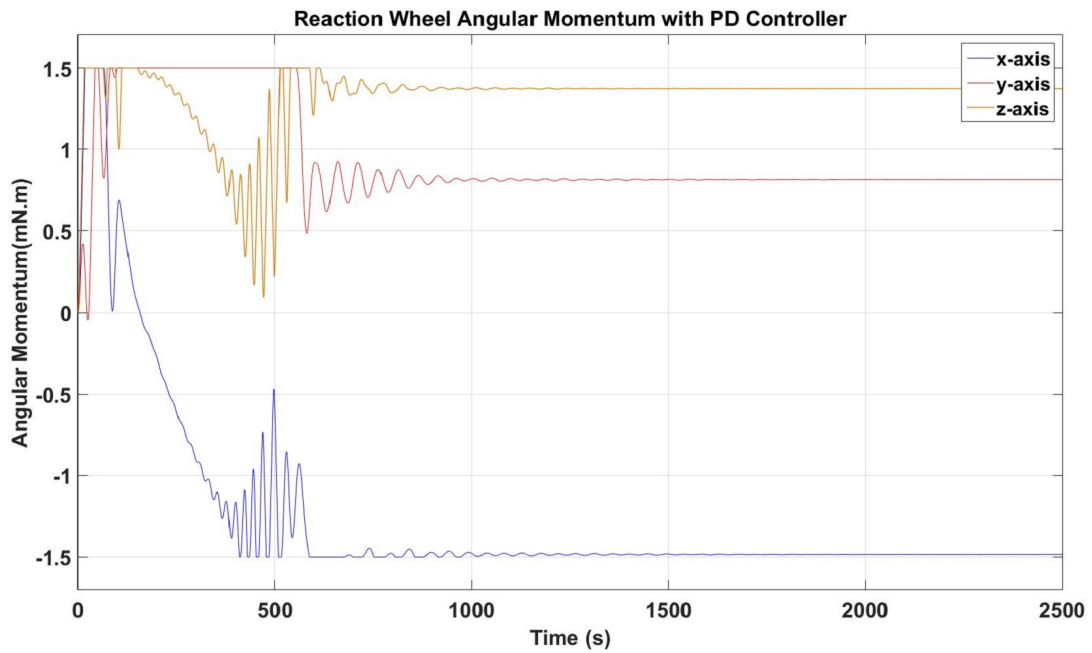


FIGURE 5.13: Angular momentum showing reaction wheels

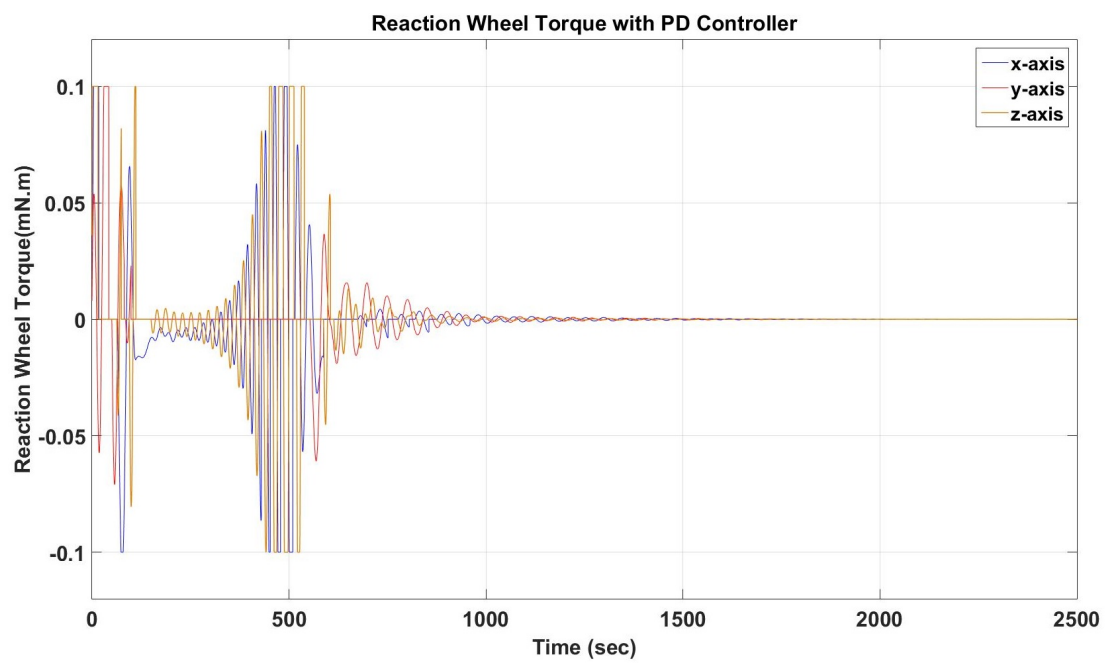


FIGURE 5.14: Reation Wheel torque response

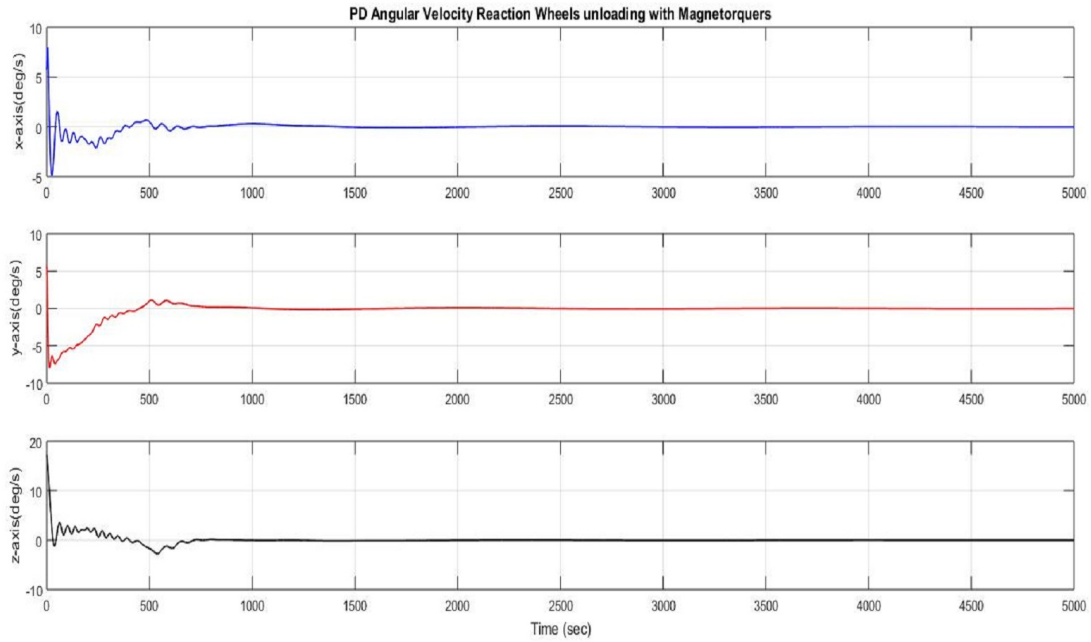


FIGURE 5.15: Angular velocity response while unloading Reaction Wheels with magnetorquers

5.3 Cross Product Control Analysis

The Cross product control law simulations were tested with the reaction wheels and magnetorquers with an initial angular velocity of the satellite $(0.1, 0.1, 0.3)rad/s$. The angular velocity of the satellite as seen in Figure 5.15 attenuates to 0 deg in all axes in about 750secs. The quaternion attitude attempts to stabilize in about 4000secs to nadir pointing mode. The angular momentum of the reaction wheel as seen in Figure 5.17 saturates in about 100secs and at the same time torque is delivered by the magnetorquers as seen in Figure 5.19 which in turn desaturates the wheels and the performance is then regulated for effective pointing.

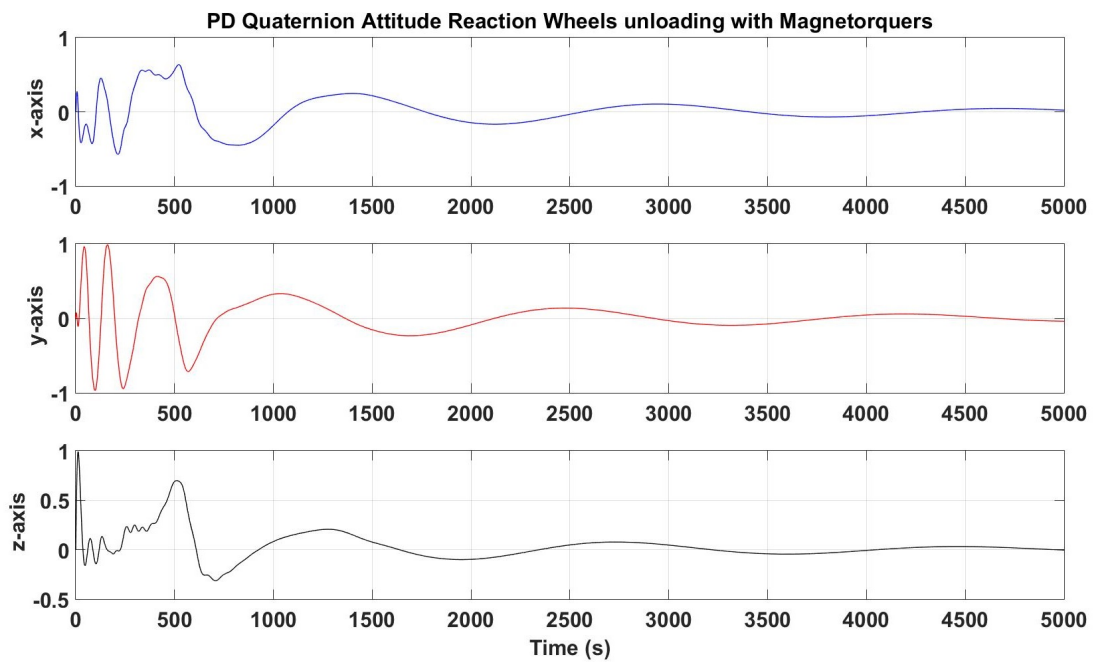


FIGURE 5.16: Quaternion Attitude during Reaction Wheel unloading with Magnetorquers

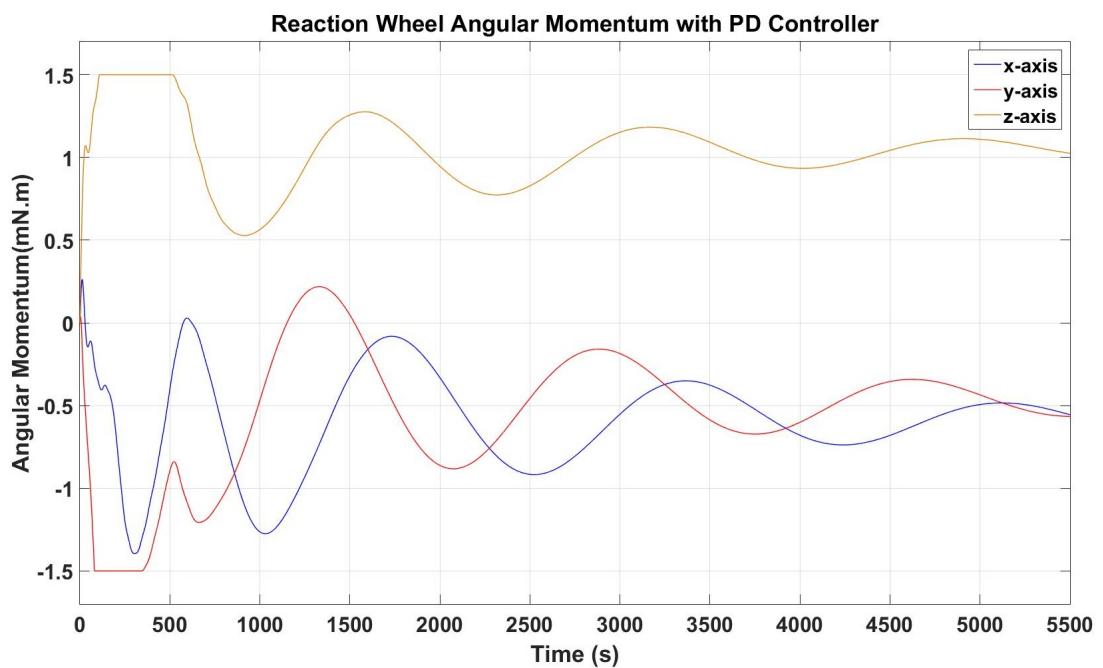


FIGURE 5.17: Reaction Wheels angular momentum saturated and unloading with magnetorquers

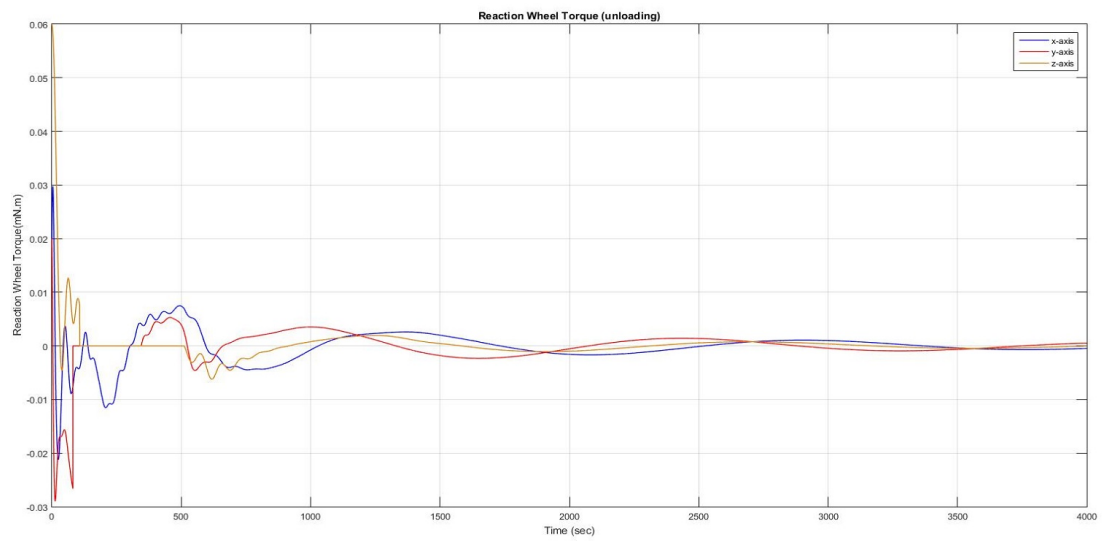


FIGURE 5.18: Reaction Wheel torque response during unloading

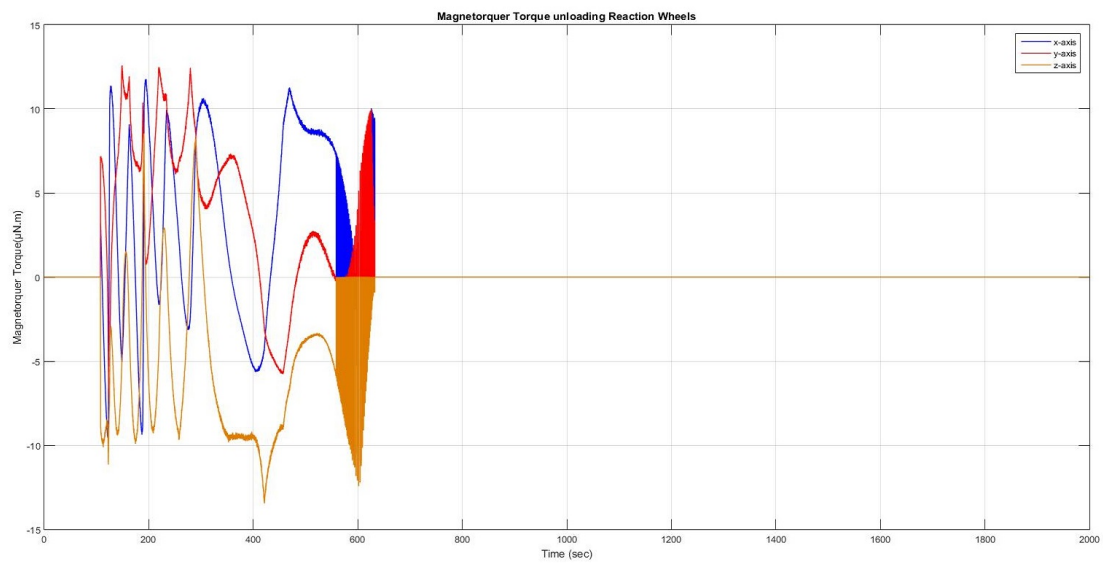


FIGURE 5.19: Magnetorquer torque response with Reaction Wheel unloading

Parameters	Values	Units
Satellite mass	4	Kg
Inertia Matrix	$J_x = 0.0331, J_y = 0.0331, J_z = 0.00678$	Kg m ²
Orbit Period T_o	5400	Sec
Orbit Angular Velocity	$\omega_o = 2\pi/T_o$	Rads/sec

TABLE 5.2: Satellite Parameters to obtain LQR controller gain.

5.4 LQR Analysis

The feedback control input defined in Equation 4.15 establishes the stability of the linearized model in a closed loop system while minimizing the cost function 4.14. In order to obtain this control input, the inertia matrix J is calculated and assumed to be diagonal as expressed in Equation 3.5. For further simplification of the design process, the weight matrices Q and R are selected to be diagonal with the number of states and number of actuator control as the lengths Q and R respectively.

$$Q = \text{diag}[Q_1, Q_2, Q_3, Q_4, Q_5, Q_6]$$

$$R = \text{diag}[R_1, R_2, R_3] \quad (5.1)$$

Q and R matrices are selected by adjusting the values and comparing the performances to the desired goal using code written in MATLAB where the feedback gain K is also calculated using the function lqr in MATLAB

$$[K, P, E] = lqr(A, B, Q, R) \quad (5.2)$$

where P is the solution of the ARE given in 4.16 and E is the closed loop eigen values $|A - BK|$ that must guarantee stability.

Figure 5.20 and 5.21 shows the step response of the system states with Q and R matrices selected as $Q = \text{diag}[1, 1, 1, 1, 1, 1]$ and $R = \text{diag}[1, 1, 1]$. The result of the closed loop Eigen values and the controller gain K are

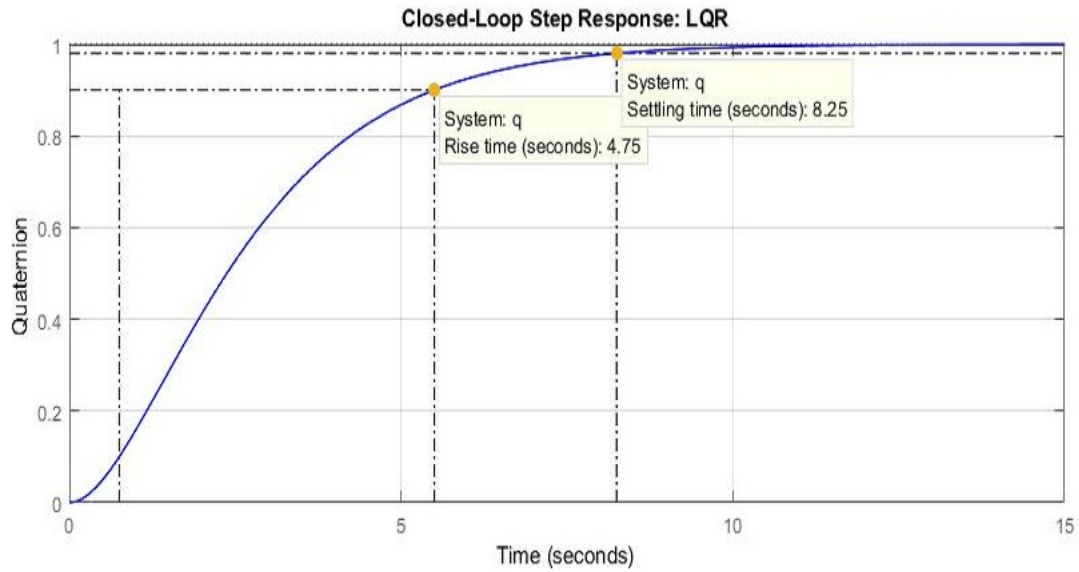


FIGURE 5.20: Quaternion Step response (weighting matrices $Q = \text{diag}[1,1,1,1,1, 1]$, $R = \text{diag}[1, 1, 1]$).

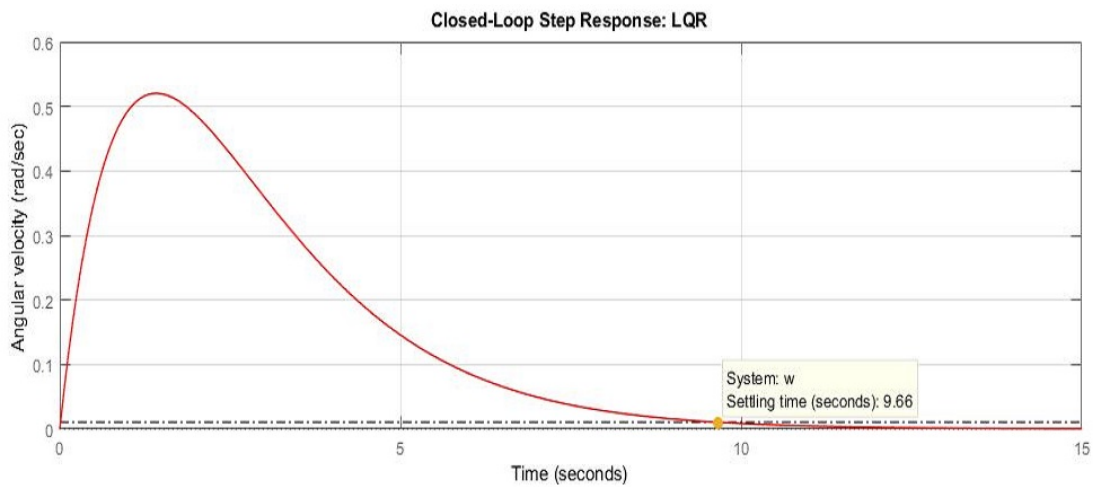


FIGURE 5.21: Angular Velocity Step response (weighting matrices $Q = \text{diag}[1,1,1,1,1, 1]$, $R = \text{diag}[1, 1, 1]$).

$$\begin{aligned}
 E &= -0.7070 + 0.0171i, -0.7070 - 0.0171i, -0.7068 + 0.0171i, \\
 &- 0.7068 - 0.0171i, -0.7071 + 0.0002i, -0.7071 - 0.0002i \\
 K &= \begin{bmatrix} 0.9977 & 0.0000 & 0.0000 & 1.4134 & 0.0000 & 0.0000 \\ 0.0000 & 1.0000 & -0.0000 & 0.0000 & 1.4142 & -0.0000 \\ -0.0000 & -0.0000 & 0.9977 & 0.0000 & -0.0000 & 1.4134 \end{bmatrix}
 \end{aligned}$$

The result of the LQR controller with reaction wheels for the purpose of precise pointing can be seen in Figures 5.22 to 5.24. The angular velocity of the satellite

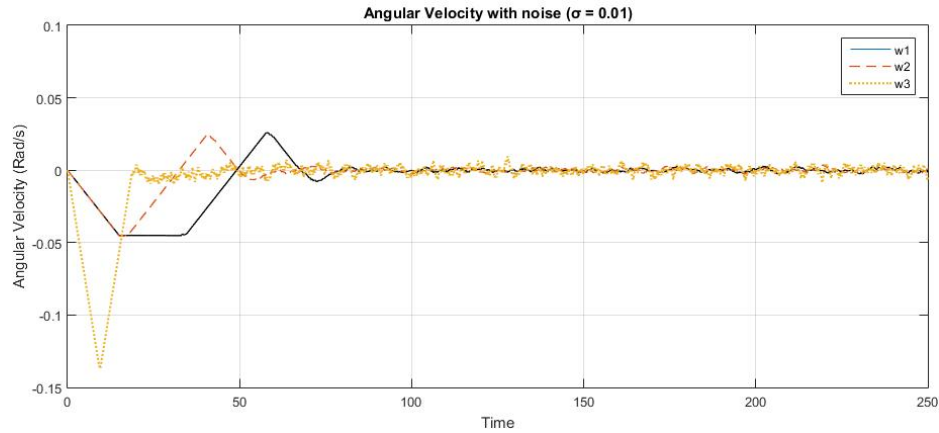


FIGURE 5.22: Angular Velocity LQR controller performance with noise.

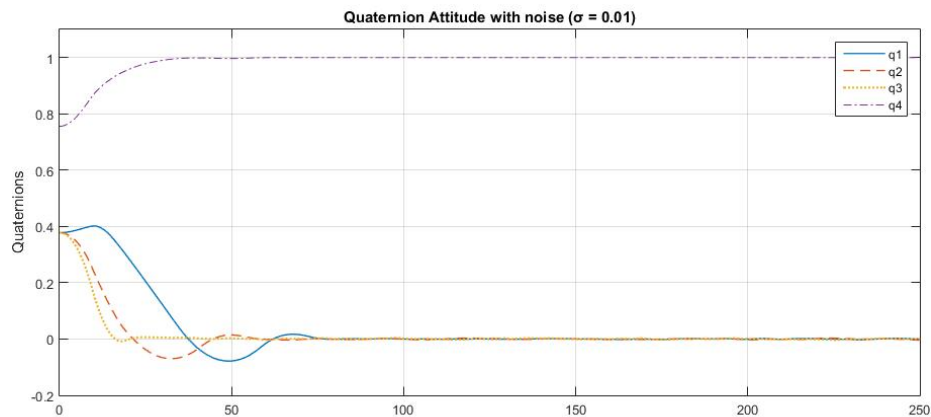


FIGURE 5.23: Quaternion Attitude LQR controller response with noise.

attenuates to zero within 100 seconds with little oscillations due to noise. The pointing requirement is satisfied as seen with 100 seconds as well.

Figures 5.25 to 5.27 shows results of the LQR controller with magnetorquers. The angular velocity of the satellite is seen to attain rest at 0 deg/s in all axes in about 1500 seconds. The controller gain was calculated with Q and R matrices selected as $Q = \text{diag}[140, 140, 140, 140, 140, 140]$ and $R = \text{diag}[2480, 2480, 2480]$. The state space model for this simulation is described in Appendix C.2

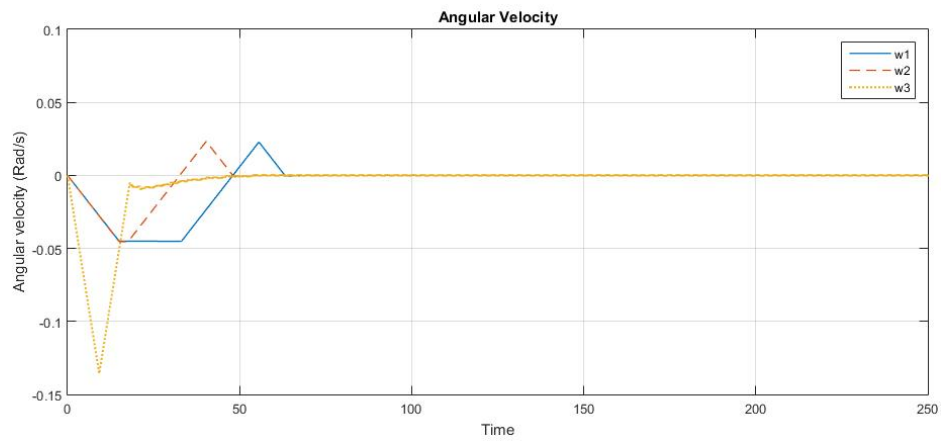


FIGURE 5.24: Angular Velocity LQR controller performance.

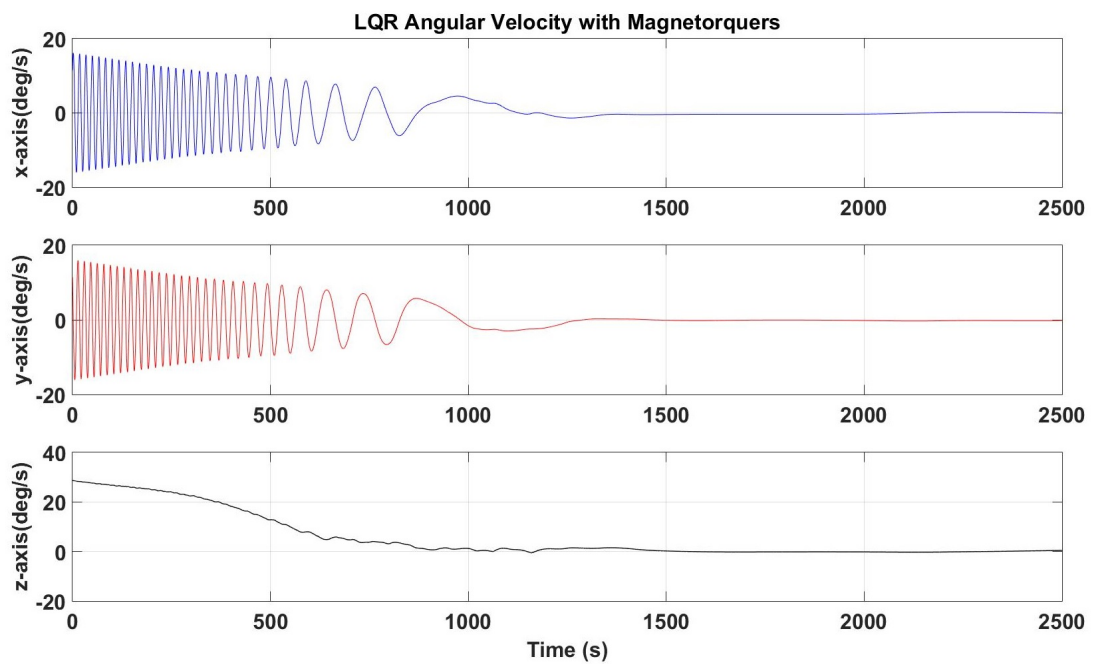


FIGURE 5.25: Angular Velocity LQR controller performance with Magnetorquers.

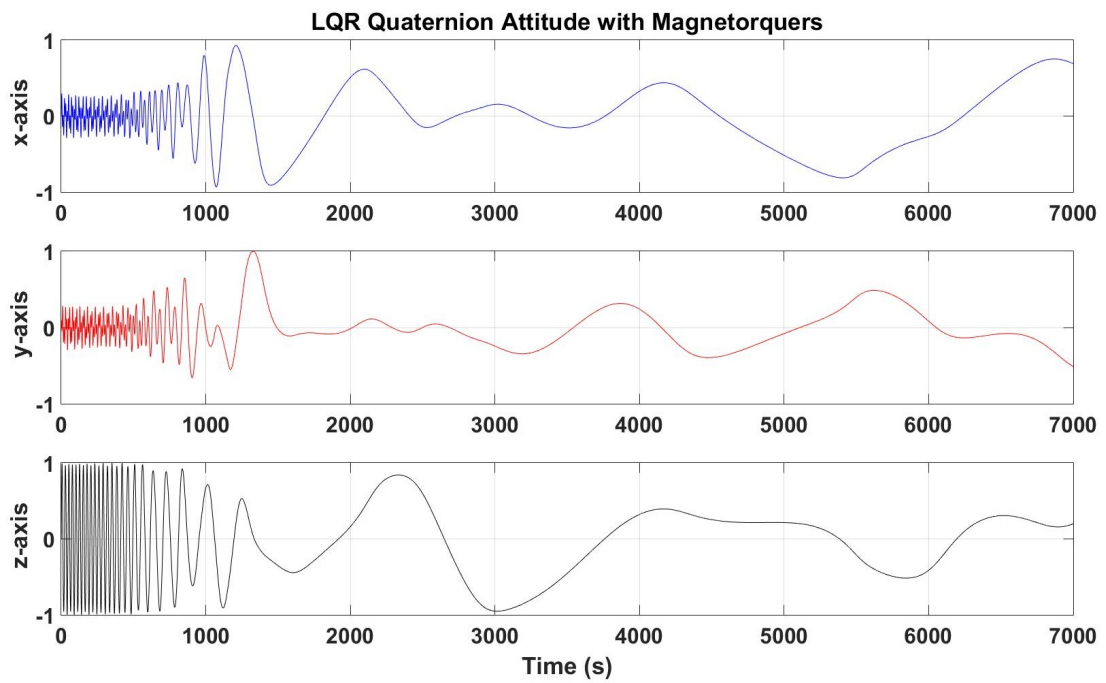


FIGURE 5.26: Quaternion Attitude LQR controller response with Magnetorquers.

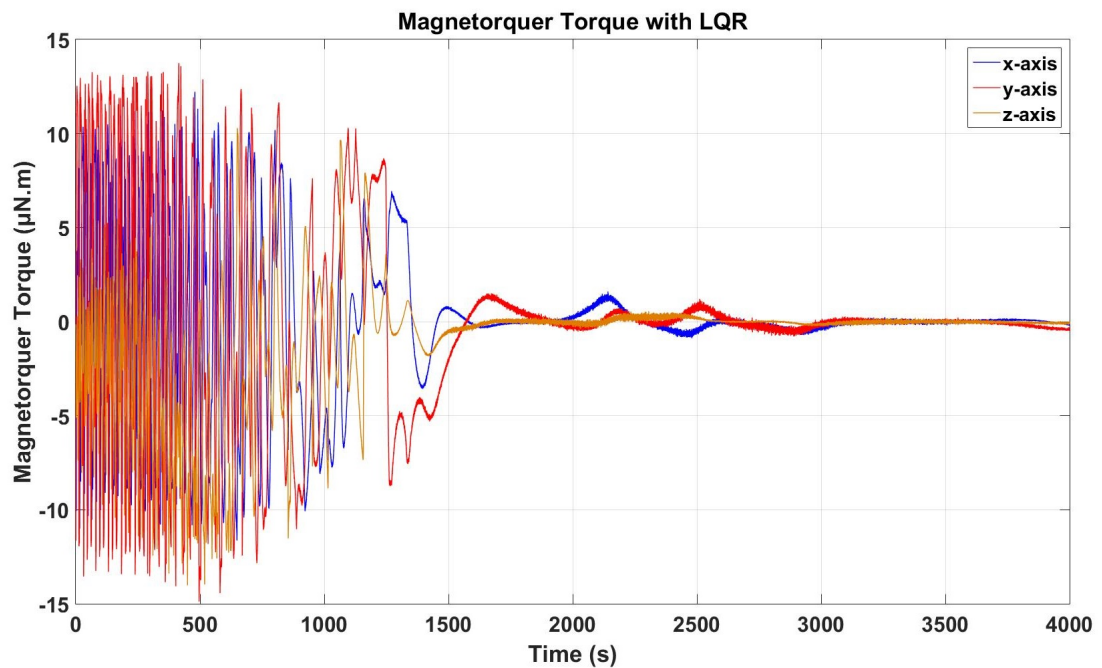


FIGURE 5.27: Magnetorquer Torque response with LQR.

Parameter	Value
Initial Angular Velocity	$(0, 0, 0)deg/s$
k	15000
k_1	0.01
Desired Angular Velocity	k_2 Gain
57 deg/s	100
115 deg/s	1000
172 deg/s	1000
230 deg/s	1000
286 deg/s	5000
360 deg/s	5000

TABLE 5.3: Spin rate simulation result.

5.5 Spin-up Controller Analysis

The Spin-up control simulation results are presented in this section with the desired ultimate angular rate set to 360 deg/s in the x-axis. As described in Section 4.5 the controller gains were set as shown in Table 5.3.

Figure 5.28 shows the angular rate of the satellite in the x-axis to about 110 deg/s while experiencing a spontaneous nutation effect. Figure 5.29 shows the angular rate spin up to about 180 deg/s, which is implemented in 2 phases to avoid a frequent nutation about the traverse axis. Figure 5.30 presents the desired angular rate which is performed in several phases and achieved in about 27 orbits as enumerated in Table 5.3

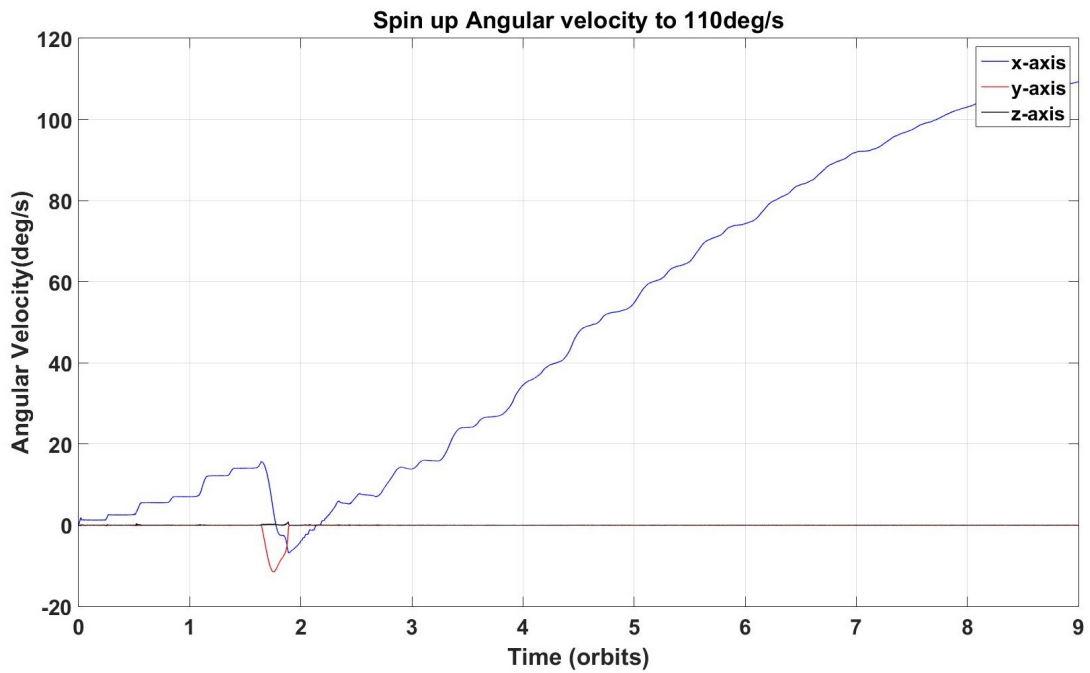


FIGURE 5.28: Angular Velocity Spin up to 110 deg/s.

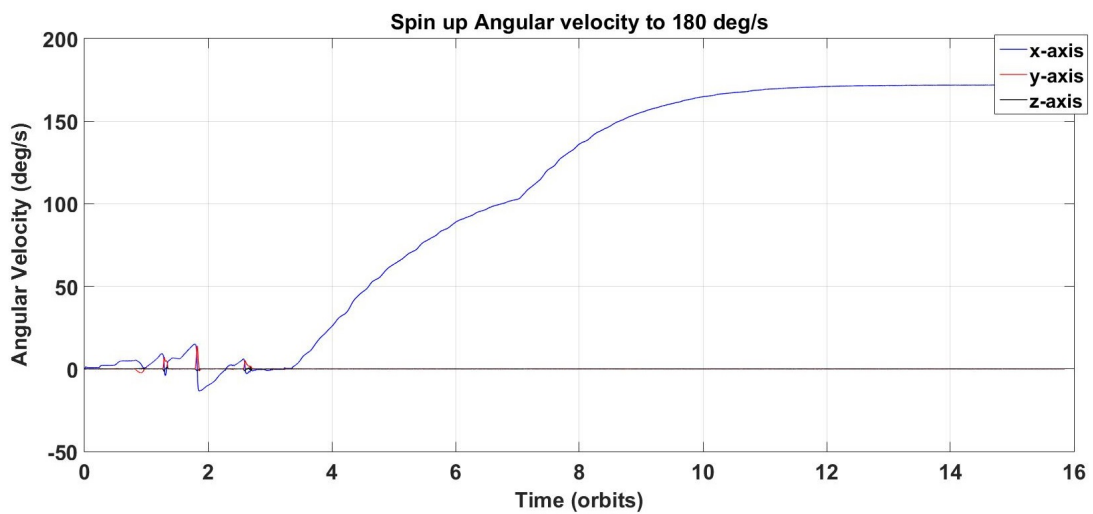


FIGURE 5.29: Angular Velocity Spin up to 180 deg/s.

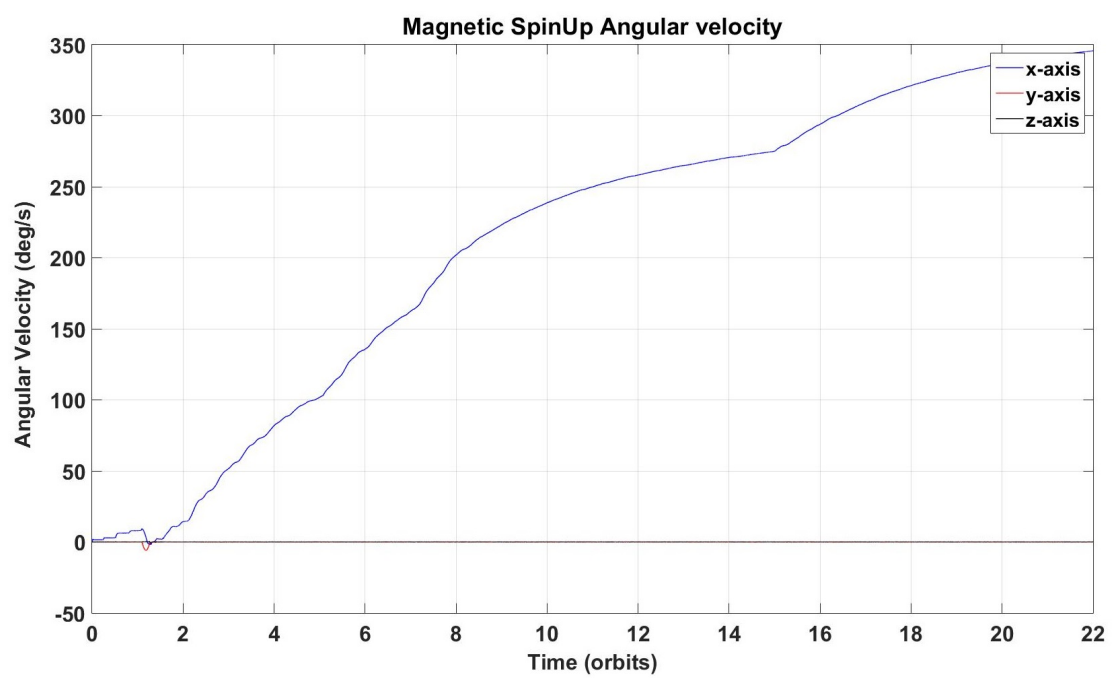


FIGURE 5.30: Angular Velocity Spin up to 360 deg/s.

6 Conclusion & Future Work

6.1 Conclusion

This thesis presented various attitude controller designs for ESTCube-2 nanosatellite. Table 6.1 gives an overview of the the various designed controllers and progress made with testing and optimization as at the time of this thesis work. Further work on these will continue to achieve specific desired requirements for the satellite mission.

Much work was done on the design of LQR optimal controller for use with the reaction wheels and magnetorquers. The LQR controller was seen to work well even with the gravity gradient disturbance torque. However, due to the influence of the Earth's magnetic field, the response with magnetorquers was not much

Control Law	Attitude Mode	Status	Future work
Bdot	Detumbling(MT)	Designed	Gain Optimisation
PD	Detumbling(MT)	Designed	
P	Detumbling(RW)	Designed	
PD	Pointing(MT)	Designed	Gain Optimisation
PD	Pointing(RW)	Designed	
Cross Product law	Wheel unloading(MT/RW)	Designed	
LQR	Pointing(MT)	Designed	Gain Optimisation
LQR	Pointing(RW)	Designed	
Angular rate control	Spin-up(MT)	Designed	Gain Optimisation
Angular rate control	Spin-up(MT/RW)	Theory Designed	Design Controller
Angular rate control	Spin-up(RW/Thruster)	Theory Designed	Design Controller

TABLE 6.1: Overview of Designed Controllers.

desirable in comparison with reaction wheels. In comparison with the PD-like control laws, LQR optimal control gave better results to stabilize the system even when realistic disturbances were added.

In order to reduce the effect of the residual dipole disturbance, ferromagnetic materials could be avoided in building the satellite.

6.2 Future Work

The control methods presented were able to attain a certain level of attitude stability based on the requirements. However much work still needs to be done to account for all necessary attitude maneuver for the ESTCube-2 mission. To attain a more efficient performance, controllers making use of the magnetorquers as actuators would require optimization in controller gain and testing of time varying gain approach. The angular rate controller for spin would also be designed for use with reaction wheels and thrusters as actuators.

The controllers designed are presented implemented in MATLAB environment, however these control algorithms would have to be written in c language and tested in simulation in SIMULINK.

Bibliography

- [1] I. Iakubivskyi, H. Ehrpais, H. Kuuste, I. Sünter, E. Ilbis, M.-L. Aru, E. Oro, J. Kütta, P. Toivanen, P. Janhunen, and A. Slavinskis, “Estcube-2 plasma brake payload for effective deorbiting,” 2017.
- [2] K. Lang, “Nasa’s cosmos,” *A space-science web site providing scientific achievements, historical background and visually appealing images. Located at the URL <http://ase.tufts.edu/cosmos>*, 2015.
- [3] S. Lätt, A. Slavinskis, E. Ilbis, U. Kvell, K. Voormansik, E. Kulu, M. Pajusalu, H. Kuuste, I. Sünter, T. Eenmäe, and others, “ESTCube-1 nanosatellite for electric solar wind sail in-orbit technology demonstration,” *Proceedings of the Estonian Academy of Sciences*, vol. 63, no. 2, p. 200, 2014.
- [4] P. Janhunen, “Electric sail for spacecraft propulsion,” *Journal of Propulsion and Power*, vol. 20, no. 4, pp. 763–764, 2004.
- [5] J. Li, M. Post, T. Wright, and R. Lee, “Design of attitude control systems for cubesat-class nanosatellite,” *Journal of Control Science and Engineering*, vol. 2013, p. 4, 2013.
- [6] S. Karataş, “Leo satellites: Dynamic modelling, simulations and some nonlinear attitude control techniques,” Master’s thesis, MIDDLE EAST TECHNICAL UNIVERSITY, 2006.

-
- [7] C. Kaplan, “Leo satellites: attitude determination and control components; some linear attitude control techniques,” Master’s thesis, MIDDLE EAST TECHNICAL UNIVERSITY, 2006.
- [8] B. W. Young, “Design and specification of an attitude control system for the dande mission,” Master’s thesis, University of Colorado at Boulder, 2008.
- [9] G. Bråthen, “Design of attitude control system of a double cubesat,” Master’s thesis, Institutt for teknisk kybernetikk, 2013.
- [10] F. G. Stray, “Attitude control of a nano satellite,” Master’s thesis, 2010.
- [11] N. Jovanovic, “Aalto-2 satellite attitude control system,” 2014.
- [12] J.-Y. Wen and K. Kreutz-Delgado, “The attitude control problem,” *IEEE Transactions on Automatic control*, vol. 36, no. 10, pp. 1148–1162, 1991.
- [13] J. D. Boškovic, S.-M. Li, and R. K. Mehra, “Robust adaptive variable structure control of spacecraft under control input saturation,” *Journal of Guidance, Control, and Dynamics*, vol. 24, no. 1, pp. 14–22, 2001.
- [14] R. J. Wallsgrove and M. R. Akella, “Globally stabilizing saturated attitude control in the presence of bounded unknown disturbances,” *Journal of Guidance, Control, and Dynamics*, vol. 28, no. 5, pp. 957–963, 2005.
- [15] Z. Zhou* and R. Colgren, “A non-linear spacecraft attitude tracking controller for large non-constant rate commands,” *International Journal of Control*, vol. 78, no. 5, pp. 311–325, 2005.
- [16] Y. Yang, “Controllability of spacecraft using only magnetic torques,” *IEEE Transactions on Aerospace and Electronic Systems*, vol. 52, no. 2, pp. 954–961, 2016.
- [17] G. Olentšenko, “Prototype design of estcube-2 attitude and orbit control system,” Master’s thesis, Tartu Ülikool, 2014.
- [18] B. Wie, H. Weiss, and A. Arapostathis, “Quarternion feedback regulator for spacecraft eigenaxis rotations,” *Journal of Guidance, Control, and Dynamics*, vol. 12, no. 3, pp. 375–380, 1989.

-
- [19] I. Iakubivskyia, H. Ehrpaisa, J. Dalbinsa, E. Orob, E. Kulub, J. Kütta, P. Janhunenc, A. Slavinskisa, E. Ilbisa, I. Plooma *et al.*, “Estcube-2 mission analysis: plasma brake experiment for deorbiting,” 2016.
- [20] W. Ley, K. Wittmann, and W. Hallmann, *Handbook of space technology*. John Wiley & Sons, 2009, vol. 22.
- [21] A. H. d. Ruiter, C. Damaren, and J. R. Forbes, *Spacecraft Dynamics and Control: An Introduction*. John Wiley & Sons, 2012, google-Books-ID: mGSYHJIIDxEC.
- [22] W. J. Larson and J. R. Wertz, “Space mission analysis and design,” 1992.
- [23] J. R. Wertz, *Spacecraft attitude determination and control*. Springer Science & Business Media, vol. 73.
- [24] M. L. Psiaki, “Magnetic torquer attitude control via asymptotic periodic linear quadratic regulation,” *Journal of Guidance, Control, and Dynamics*, vol. 24, no. 2, pp. 386–394, 2001.
- [25] J. R. Wertz and W. J. Larson, “Space mission analysis and design,” 1999.
- [26] A. Slavinskis, M. Pajusalu, H. Kuuste, E. Ilbis, T. Eenmäe, I. Sünter, K. Laizans, H. Ehrpais, P. Liias, E. Kulu *et al.*, “Estcube-1 in-orbit experience and lessons learned,” *IEEE Aerospace and Electronic Systems Magazine*, vol. 30, no. 8, pp. 12–22, 2015.
- [27] H. Ehrpais, J. Kütt, I. Sünter, E. Kulu, A. Slavinskis, and M. Noorma, “Nanosatellite spin-up using magnetic actuators: Estcube-1 flight results,” *Acta Astronautica*, vol. 128, pp. 210–216, 2016.
- [28] A. A. White and R. Bromley, “Dynamically consistent, quasi-hydrostatic equations for global models with a complete representation of the coriolis force,” *Quarterly Journal of the Royal Meteorological Society*, vol. 121, no. 522, pp. 399–418, 1995.
- [29] H. Ehrpais, I. Sünter, E. Ilbis, J. Dalbins, I. Iakubivskyi, E. Kulu, I. Ploom, P. Janhunen, J. Kuusk, J. Šate, and others, “ESTCube-2 mission and satellite design,” in *The 4S Symposium*, 2016.

-
- [30] J.-F. Tréguët, D. Arzelier, D. Peaucelle, C. Pittet, and L. Zaccarian, “Reaction wheels desaturation using magnetorquers and static input allocation,” *IEEE Transactions on Control Systems Technology*, vol. 23, no. 2, pp. 525–539, 2015.
- [31] X. Chen, W. H. Steyn, S. Hodgart, and Y. Hashida, “Optimal combined reaction-wheel momentum management for earth-pointing satellites,” *Journal of guidance, control, and dynamics*, vol. 22, no. 4, pp. 543–550, 1999.
- [32] B. Kim, H. Lee, and S. Choi, “Three-axis reaction wheel attitude control system for kitsat-3 microsatellite,” *Space Technology*, vol. 5, no. 16, pp. 291–296, 1996.
- [33] R. Reynolds and G. Creamer, “Global lyapunov control of spin stabilized spacecraft,” in *2001 Flight Mechanics Symposium*, vol. 1, 2001.
- [34] A. de Ruiter, “A fault-tolerant magnetic spin stabilizing controller for the jc2sat-ff mission,” *Acta Astronautica*, vol. 68, no. 1, pp. 160–171, 2011.
- [35] M. Blanke and M. B. Larsen, “Satellite dynamics and control in a quaternion formulation,” Technical University of Denmark, Department of Electrical Engineering, Tech. Rep., 2010.
- [36] Y. Yang, “Quaternion based model for momentum biased nadir pointing spacecraft,” *Aerospace Science and Technology*, vol. 14, no. 3, pp. 199–202, 2010.

A Controllability Analysis

For a linear system given as

$$\dot{x}(t) = Ax(t) + Bu(t) \quad (\text{A.1})$$

the system is said to be controllable if for all initial conditions $x(t_0)$, final conditions $x(t_f)$ and where $t_f > 0$, there would exist a control input $u(t)$, in the range $0 < t < t_f$ such that

$$x(t) = x(t_f)$$

In other words, the Controllability property is aimed to find $u(t)$ such that the states are forced to go from an initial state, $x(t_0)$ to a final desired state $x(t_f)$ in a finite time period.

The controllability condition states that the state and input matrix, A,B, satisfy that

$$C_o = [B|AB|A^2B|\dots|A^{n-1}B] \quad (\text{A.2})$$

where n is the dimension of A and the system is therefore controllable if and only if C_o has a full rank, $\text{rank}(C_o) = n$. The controllability of the designed system is determined by using Matlab controllability function $\text{ctrb}()$.

B Linear Programming Code.

LQR Gain with Reaction Wheels

```
InertiaM =[0.0331, 0, 0; 0, 0.0331, 0; 0, 0, 0.00678];

T_o = 90*60; %sec
omega_o = 2*pi/T_o;
omega_o_sq = omega_o*omega_o;

%RW_h = [1;1;1];

f_41 = 8*(InertiaM(3,3) - InertiaM(2,2))*omega_o_sq - 2*omega_o;
f_46 = (-InertiaM(1,1) -InertiaM(3,3) + InertiaM(2,2))*omega_o ;
f_52 = 6*(InertiaM(3,3) - InertiaM(1,1))*omega_o_sq;
f_63 = 2*(InertiaM(1,1) - InertiaM(2,2))*omega_o_sq - 2*omega_o;
f_64 = -(f_46);

%qBI = (qBI(1:3));
%x = [qBI; RotVel_B];

Adr = zeros(3);
Adr(1,3) = f_46;
Adr(3,1) = f_64;
```

```

Ad1 = zeros(3);
Ad1(1,1) = f_41; Ad1(2,2) = f_52; Ad1(3,3) = f_63;
Au = [zeros(3) eye(3)*0.5];
Ad = [Ad1 Adr];
A = [Au; Ad];

```

```
B = [zeros(3); eye(3)];
```

```
Q = diag([1,1,1,1,1,1]);
```

```
R = diag([1,1,1]);
```

```
%K = [31.066 0 0 0.7905 0 0;...
```

```
% 0 41.7118 0 0 0.7905 0;...
```

```
% 0 0 49.5115 0 0 0.7905];
```

```
[K,p,e] = lqr(A,B,Q,R)
```

LQR Gain with Magnetorquers

```
InertiaM=[0.0331, 0, 0; 0, 0.0331, 0; 0, 0, 0.00678];
```

```
T_o = 90*60; %sec
```

```
omega_o = 2*pi/T_o;
```

```
omega_o_sq = omega_o*omega_o;
```

```
f_41 = (8*(InertiaM(3,3) - InertiaM(2,2))*omega_o_sq)/InertiaM(1,1);
```

```
f_46 = ((-InertiaM(1,1) -InertiaM(3,3) + InertiaM(2,2))*omega_o)/InertiaM(1,1);
```

```
f_52 = (6*(InertiaM(3,3) - InertiaM(1,1))*omega_o_sq)/InertiaM(2,2);
```

```
f_63 = (2*(InertiaM(1,1) - InertiaM(2,2))*omega_o_sq)/InertiaM(3,3);
```

```
f_64 = ((InertiaM(1,1) +InertiaM(3,3) -InertiaM(2,2))*omega_o)/InertiaM(3,3);
```

```
%qBI = (qBI(1:3));
```

```
%x = [qBI; RotVel_B];
```

```
Adr = zeros(3);
Adr(1,3) = f_46;
Adr(3,1) = f_64;
Adl = zeros(3);
Adl(1,1) = f_41; Adl(2,2) = f_52; Adl(3,3) = f_63;
Au = [zeros(3) eye(3)*0.5];
Ad = [Adl Adr];
A = [Au; Ad];

B = [zeros(3); 0 0 (3.6838e-05)/InertiaM(1,1); 0 0 0;...
     (-3.6838e-05)/InertiaM(3,3) 0 0];

Q = diag([140,140,140,140,140,140]);
R = diag([2480,2480,2480]);

%K = [31.066 0 0 0.7905 0 0;...
%     0 41.7118 0 0 0.7905 0;...
%     0 0 49.5115 0 0 0.7905];

[K,p,e] = lqr(A,B,Q,R)
```

C Nadir Pointing Satellite Model

With Reaction Wheels

C.1 Model with Reaction Wheels

The linearization of the satellite model was described in Section 3.6, here the satellite model is described with respect to nadir pointing of the satellite with reaction wheels. The dynamic model representing the satellite with reaction wheels is given below as described in [35].

$$J\dot{\omega}_i = T_d + T_c - \Omega(\omega_i)(J\omega_i + H) \quad (\text{C.1})$$

where $H = [h_1 h_2 h_3]^T$ is the angular momentum of the wheel. Here, the Nadir pointing Attitude is represented by the SBRF rotation to the orbit frame (LVLH). The transformation matrix representing the orbit frame to the SBRF is A_o^B . therefore the angular velocity of the satellite in the inertial reference frame is given as

$$\omega_i = \omega + A_o^B \omega_o = \omega + \omega_o^B \quad (\text{C.2})$$

ω is described as the angular velocity in the body frame with respect to the orbit frame. The derivative is also obtained as give below with $\dot{\omega}_o$ regarded as small and negligible.

$$\dot{\omega}_i = \dot{\omega} + \dot{A}_o^B \omega_o + A_o^B \dot{\omega}_o = \dot{\omega} - \omega \times \omega_o^B \quad (\text{C.3})$$

Therefore, Equation C.1 can be re-written as

$$J\dot{\omega}_i = T_d + T_c - \Omega(\omega + \omega_o^B)(J(\omega + \omega_o^B) + H) \quad (\text{C.4})$$

This can further be expressed with the angular momentum quite small and negligible.

$$J\dot{\omega}_i = T_d + T_c + f(\omega, \omega_o^B) \quad (\text{C.5})$$

For nadir pointing of the satellite, the satellite angular velocity rate in SBRF with respect to orbit frame should be as small as possible $\omega \approx 0$ and both frames be aligned with very little error $q_1, q_2, q_3 = 0$. Also, we consider the orbit rate of the satellite in a circular orbit $\omega_o = 2\pi/T_o$. The linearized nadir pointing model in state space form of $\dot{x} = Ax + BT_c$ with gravity gradient torque is given as described in [36]

$$\begin{bmatrix} \dot{q} \\ \dot{\omega}_i \end{bmatrix} = \begin{bmatrix} 0 & 0 & 0 & 0.5 & 0 & 0 \\ 0 & 0 & 0 & 0 & 0.5 & 0 \\ 0 & 0 & 0 & 0 & 0 & 0.5 \\ f_{41} & 0 & 0 & 0 & 0 & f_{46} \\ 0 & f_{52} & 0 & 0 & 0 & 0 \\ 0 & 0 & f_{63} & f_{64} & 0 & 0 \end{bmatrix} \begin{bmatrix} q \\ \omega_i \end{bmatrix} + \begin{bmatrix} 0 & 0 & 0 \\ 0 & 0 & 0 \\ 0 & 0 & 0 \\ 1 & 0 & 0 \\ 0 & 1 & 0 \\ 0 & 0 & 1 \end{bmatrix} (T_c) \quad (\text{C.6})$$

where

$$f_{41} = 8(J_{33} - J_{22})\omega_o^2 - 2\omega_o$$

$$f_{46} = (-J_{11} - J_{33} + J_{22})\omega_o$$

$$f_{52} = 6(J_{33} - J_{11})\omega_o^2$$

$$f_{63} = 2(J_{11} - J_{22})\omega_o^2 - 2\omega_o$$

$$f_{64} = -f_{46}$$

C.2 Model with Magnetorquers

The initial model is same as that used in the previous section, however, the control torque used is that generated by the magnetic coil also described in 2.5.2 where $T_c = m \times b$.

The magnetic field b is also expressed based on the dipole model described in Section 3.3.1 as

$$b = \begin{bmatrix} b_1(t) \\ b_2(t) \\ b_3(t) \end{bmatrix} = \frac{\mu_f}{a^3} \begin{bmatrix} \cos \omega_0 t \sin \theta \\ -\cos \theta \\ 2 \sin \omega_0 t \sin \theta \end{bmatrix} \quad (\text{C.7})$$

With the inclination of the spacecraft orbit and the magnetic equator $\theta = 0$ the quaternion linear time invariant model is therefore reduced and given by [16]

$$\begin{bmatrix} \dot{q} \\ \dot{\omega}_i \end{bmatrix} = \begin{bmatrix} 0 & 0 & 0 & 0.5 & 0 & 0 \\ 0 & 0 & 0 & 0 & 0.5 & 0 \\ 0 & 0 & 0 & 0 & 0 & 0.5 \\ f_{41} & 0 & 0 & 0 & 0 & f_{46} \\ 0 & f_{52} & 0 & 0 & 0 & 0 \\ 0 & 0 & f_{63} & f_{64} & 0 & 0 \end{bmatrix} \begin{bmatrix} q \\ \omega_i \end{bmatrix} + \begin{bmatrix} 0 & 0 & 0 \\ 0 & 0 & 0 \\ 0 & 0 & 0 \\ 0 & 0 & -b_2/J_{11} \\ 0 & 0 & 0 \\ -b_2/J_{33} & 0 & 0 \end{bmatrix} \begin{bmatrix} m_1 \\ m_2 \\ m_3 \end{bmatrix} \quad (\text{C.8})$$

where

$$\begin{aligned} f_{41} &= 8 \frac{(J_{33} - J_{22})}{J_{11}} \omega_o^2 \\ f_{46} &= \frac{(-J_{11} - J_{33} + J_{22})}{J_{11}} \omega_o \\ f_{52} &= 6 \frac{(J_{33} - J_{11})}{J_{22}} \omega_o^2 \\ f_{63} &= 2 \frac{(J_{11} - J_{22})}{J_{33}} \omega_o^2 \\ f_{64} &= \frac{(J_{11} + J_{33} - J_{22})}{J_{33}} \omega_o \end{aligned}$$

D Abstracts Accepted for Oral Presentations

D.1 Abstract for 68th International Astronautical Congress 2017 - *Tether Deployment Using High Spin Rate Control For Interplanetary Nanosatellite Missions*

This paper presents a high spin rate control algorithm based on a Linear Quadratic Regulator (LQR) used for tether deployment on the ESTCube-2 3U nanosatellite. The 300m long tether, consisting of 4 parallel $25\mu\text{m}$ diameter wires, will be deployed using centrifugal force generated by spinning up the satellite. The deployed tether will be used for a deorbiting experiment employing the plasma break technology. The attitude control system of ESTCube-2 will use electromagnetic coils, reaction wheels and cold gas thrusters as actuators. The LQR will be designed based on linearized satellite dynamics. The aim of the controller is to spin up the satellite to 360 deg/s about the X-axis (short axis) while simultaneously aligning the spin axis with the Earth's polar axis. The paper will also describe the design of an LQR optimal controller with controllability and stability analysis to meet the strict pointing requirements of the ESTCube-2 Earth observation camera and the high speed communication antenna. The simulation results will be presented and analysed to improve controller performance. The attitude control

algorithms will be flight tested on ESTCube-2 as a stepping stone for ESTCube-3 which is planned to be launched to lunar orbit.

D.2 Abstract for 6th iCubeSat Workshop 2017 - *ESTCube-2 Nanosatellite Attitude Control for Interplanetary Missions*

This paper presents the design and study of attitude control algorithms for the ESTCube-2/3 missions making use of electromagnetic coils, reaction wheels and cold gas thrusters as actuators. The controllers designed are based on fulfilling the set requirements of the ESTCube-2 mission. The 3U CubeSat is required to spin up for the centrifugal tether deployment for the Plasma Brake experiment. The algorithm designed for this is required to spin the satellite up to 360 deg/s about the X-axis while simultaneously ensuring the alignment of the satellite with Earth's polar axis. The attitude control system is designed to also satisfy the strict pointing requirement of which a Linear Quadratic Regulator controller (LQR) has been designed with controllability and stability analysis based on linearized satellite dynamics and is being enhanced for tracking making use of the reaction wheels of the satellite. In addition, we present attitude control methods to be tested for the ESTCube-3 which is meant for the lunar orbit applying a combination of reaction wheels and cold gas thrusters for attitude maneuvering. Results based on simulations are therefore presented and analyzed for improved performance.

Non-exclusive licence to reproduce thesis and make thesis public.

I, **Ikechukwu Ofodile** (date of birth: 31.08.1993),

1. herewith grant the University of Tartu, Estonia a free permit (non-exclusive license) to:

1.1. reproduce, for the purpose of preservation and making available to the public, including for addition to the DSpace digital archives until expiry of the term of validity of the copyright, and

1.2. make available to the public via the web environment of the University of Tartu, including via the DSpace digital archives until expiry of the term of validity of the copyright,

Design and Comparison of Attitude Control Modes for ESTCube-2

supervised by Dr. Andris Slavinskis and Assoc. Prof. Gholamreza Anbarjafari

2. I am aware of the fact that the author retains these rights.

3. I certify that granting the non-exclusive licence does not infringe the intellectual property rights or rights arising from the Personal Data Protection Act.

Tartu 17.05.2017
